Durham E-Theses

Spectroscopic ellipsometry on thin films of conjugated polymers

Tammer, Michael

How to cite:

Tammer, Michael (2001) *Spectroscopic ellipsometry on thin films of conjugated polymers*, Durham theses, Durham University. Available at Durham E-Theses Online: http://etheses.dur.ac.uk/3768/

Use policy

Spectroscopic Ellipsometry on Thin Films of

Conjugated Polymers

Michael Tammer

A thesis submitted to the University of Durham

Department of Physics

for the degree of Master of Science

2001

Abstract

This work presents results from spectroscopic ellipsometry measurements of thin films of conjugated polymers constructed by spin casting with rapid solvent evaporation. Accurate data for the optical functions of MEH-PPV, PF2/6am5, PPy and PmPy films are given for the first time in a broad spectral range. A uniaxial anisotropic character is present in these functions with the optical axis parallel to the surface normal. The amount of anisotropy is found to be fairly high even in polymer layers with less rigid rod molecule chains (PF2/6am5 and MEH-PPV) and very high for the highly π-stiff polymer PPy.

The influence of an anisotropic and highly dispersive optical response on the efficiency of light emitting diodes made from PF2/6am4 is investigated. The out-coupling efficiency in such devices is found to be highly dependent on the emission wavelength. The results obtained are compared to the commonly used approximation $n = \mathrm{const.} = 2$. The importance of a proper knowledge of the optical behavior of this material group when utilized in devices is shown by the significant difference between these methods.

The ability of ellipsometry to monitor structural changes in conjugated polymers is demonstrated. The perfect rigid rod behavior of PPy and the loss of rigidity when forming a copolymer together with *meta* mPy is clearly visible in the ellipsometry data. The amount of anisotropy is dependent of the ratio of mPy and an isotropic respond is obtained for pure PmPy. Furthermore, the blue shifted absorption spectrum for higher ratios of PmPy validate breaks in the conjugation by the additional meta linkages in the chain.

Contents

List of Figures

List of Polymers

- MEH-PPV

   $poly(2-methoxy, 5-(2'-ethyl-hexyloxy)-p-phenylenevinylene)$

Fig. 1: Chemical structure of MEH-PPV

- PPy

   $poly(2, 5-pyridinediyl)$
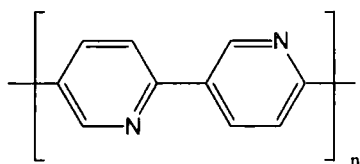
Fig. 2: Chemical structure of PPy

● PmPy

$poly(2, 6 - pyridinediyl)$
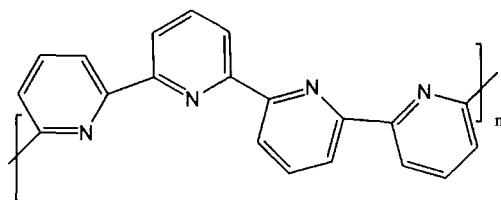
Fig. 3: Chemical structure of PmPy

● PF2/6am4

$\alpha, \omega - Bis[N, N - di(4 - methylphenyl)aminophenyl] - poly(9, 9 - bis(2 - ethylhexyl)fluoren - 2, 7 - diyl)$
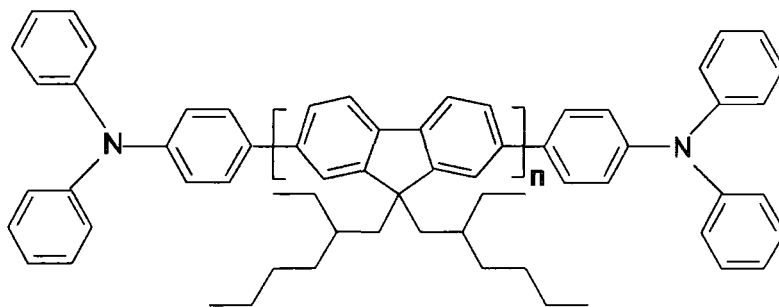
Fig. 4: Chemical structure of PF2/6am4

Declaration

The material contained in this thesis has not been submitted for the examination for any other degree, or part thereof at the University of Durham or any other institution. The material contained in this thesis is the work of the author except where formally acknowledged by reference.

Acknowledgments

First I would like to thank Dr. Andy Monkman for being an excellent supervisor. His guidance and advise during this year is highly appreciated. Another big thankyou goes to all members of his group for helping a newbie in the research business. Thank you Roger Higgins, Corin Sitch, Georgios Tzamalis, Dr. Navied Zaid and all the other people who gave me a warm welcome here.

I am especially grateful to my parents and my whole family. Without their great support I wouldn't be this far now. But also their financial backup made all this possible. Furthermore, I thank Dr.-Ing. Erich Müller Stiftung for funding.

Norman and Dave deserve gratefulness for solving all the smaller and bigger problems in everyday research live and providing me with everything I wanted. Thanks to John Gibson for the supply of silicon wafer. I also want to thank the people from the electronic workshop for fixing the monochromator for me. For the supply of all the different polymers I want to thank Dr. Lockhart Horsburgh (PPy), Covion (MEH-PPV) and Max Planck institute for polymer research (PFO).

I am very much obliged to the one, who came up with the idea of putting a firewall around the university network. Without this person I would probably still play online games instead of finishing my thesis. However, thank you Betty, Eejit, Eric, L and Lardinator, that I could play CS, TO and UT with you guys instead.

I also want to say thankyou to Carsten Rothe for pushing me to start with him this little adventure and Frank Feller for pushing us both.

Publications resulting from this work

1. M. Tammer, A. P. Monkman; Measurement of the anisotropic refractive indices of spin cast thin poly(2-methoxy,5-(2'-ethyl-hexyloxy)-p-phenylenevinylene) (MEH-PPV) films. *Advanced Materials* **2002, Accepted**

2. M. Tammer, R.W.T. Higgins and A.P.Monkman; High optical anisotropy in thin films of polyfluorene and its affect on the out-coupling of light in typical polymer light emitting diode structures. *Applied Physics*, **Accepted**

3. M. Tammer, L. Horsburgh, A. P. Monkman, W. Brown and H. D. Burrows; Effect of chain rigidity and effective conjugation length on the structural and photophysical properties of pyridine-based luminescent polymers. *Advanced Functional Materials*, **Accepted**

Chapter 1

Introduction

Since the first observation of electroluminescence in the conjugated polymer poly(phenylene vinylene) (PPV) in 1990 [1], a wide range of potential applications have been arisen for this material group in the optics sector, e.g. polymer light emitting diodes (PLEDs), photovoltaic devices and microcavity polymer laser [2, 3]. The development of thin-film devices allowed sufficient high field gradients in the polymer layer necessary for light emission which is the requirement for the application of these organic materials as a low-price replacement for inorganic semiconductors in such devices. First products have already found their way into our life in form of car radio and cell phone displays. There are various advantages of conjugated polymers in their application in light emitting devices like the flexibility of sample preparation [4] and a wide range of emission colors including the important visible region of the spectrum [5]. Other than for inorganic semiconductors the usage of polymers will redundantize the need of a high quality clean room atmosphere and sensitive, precise and therefore expensive instruments in the production process.

For the design of high efficient devices it is important to know the optical

1

properties of the polymer like index of refraction or dielectric function. These properties are expected to be different in thin films, which are used in applications, compared to bulk samples or solutions. A measurement technique designed for investigating this type of structure is therefore essential for the research in this field. Ellipsometry as a powerful, non-destructive and very sensitive tool experienced an increasing popularity in the last thirty years especially for investigations of inorganic semiconductor layers. The recent development in this measurement technique in form of variable angle spectroscopic ellipsometry (VASE) together with the fast increasing computer power, available today for the analysis of the data, enables it finally to determine even the complex optical behavior in layer structures of conjugated polymers, where a high anisotropic and dispersive respond has to be assumed in the general case.

In chapter 4, after the presentation of the necessary theoretical background in chapter 2 and a detailed description of the applied experimental techniques in chapter 3, VASE is introduced with measurements of the commonly used conjugated polymer MEH-PPV and the advantages provided by this novel method are pointed out. Accurate anisotropic dispersion data for this material is shown for the first time in a broad spectral range. The degree of anisotropy in this data is analyzed and conclusions about chain conformation in thin films are drawn from these results.

The optical functions of another important polymer, PF2/6am5, are presented in chapter 5 and used to investigate the consequences of the optical behavior for applications in PLEDs. For devices made from PF2/6am4, the connection between structural property with the resulting optical respond and the actual efficiency of the PLED is calculated. It is presented how the knowledge of the complex index of refraction can be used to improve

the amount of light able to couple out of the device and is therefore useful for applications. Furthermore, indications for a possible misguidance in the understanding of the internal processes in PLEDs because of a too coarse approximation of the refractive index, very often used in past publications, are found.

The chapter 6 of this thesis concentrates on the ability of VASE measurements to visualize changes in the structure of the conjugated polymer PPy by exploiting the changed photophysical properties. A new *meta* PmPy polymer type was created by Lockhart Horsburgh with the goal to break the conjugation length and obtain a blue shifted emission. By controlling the ratio of the monomeric components of PPy and PmPy in the synthesis of a copolymer based on these materials, effective conjugation length and chain rigidity is affected and this is clearly visible in the data provided by VASE. The presented dispersion data of different copolymers features a blue shifted absorbtion band for higher ratios of PmPy and a variation in the amount of anisotropy in the optical functions of these materials. This positive feedback about the success of the desired effect allows to optimize the tuning of the light emitting material.

Chapter 2

Theory

2.1 Electromagnetic Waves and Matter

2.1.1 Definition of Waves and Optical Functions

The Interaction between electromagnetic radiation and matter has become a very important field in the study of conjugated polymers due to the location of the absorption band of these substances in the well accessible range between infrared and ultraviolet wavelengths. The Maxwell equations [6] can be used to describe the propagation of electromagnetic waves and their interaction with matter.

$$\nabla \times \vec{H} = \frac{\partial \vec{D}}{\partial t} + \vec{J} \tag{2.1}$$

$$\nabla \times \vec{E} = -\frac{\partial \vec{B}}{\partial t} \tag{2.2}$$

$$\nabla \cdot \vec{D} = \rho \tag{2.3}$$

$$\nabla \cdot \vec{B} = 0 \tag{2.4}$$

The quantity ρ is the electric charge density. The electric field vector $\vec{E}$ and the current density $\vec{J}$, the same field vector also together with the electric

displacement vector $\vec{D}$ and the magnetic field vector $\vec{H}$ with the magnetic induction vector $\vec{B}$ are all connected by tensors of rank 2. These three material equations are necessary to describe the relation between field and matter completely.

$$\vec{D} = \varepsilon_0 \hat{\varepsilon} \vec{E} \tag{2.5}$$

$$\vec{B} = \mu_0 \hat{\mu} \vec{H} \tag{2.6}$$

$$\vec{J} = \hat{\sigma} \vec{E} \tag{2.7}$$

The dielectric tensor $\hat{\varepsilon}$ and magnetic permeability tensor $\hat{\mu}$ describe the macroscopic response of matter. In free space, only the constants electrical permittivity ε_0 and the magnetic permeability μ_0 are of interest ($\hat{\mu} = \hat{\varepsilon} = \mathbf{1}$). The combination of the Maxwell equations with the material equations yields a differential expression every wave equation has to fulfil:

$$\nabla^2 \vec{E} - \frac{1}{c^2} \frac{\partial^2 \vec{E}}{\partial t^2} = 0. \tag{2.8}$$

One solution of the electric field wave equation is the plane wave:

$$\vec{E}(\vec{r}, t) = \vec{E}_0 \, \exp\left(-i \, \vec{q} \cdot \vec{r}\right) \exp(-i\omega t) \tag{2.9}$$

where ω is the angular frequency of the wave and $\vec{q}$ the complex wave vector with $q^2 = \omega^2 \hat{\varepsilon} \mu_0$. The propagation of the wave is along the direction of $\vec{q}$. For propagation in vacuum the dielectric tensor $\hat{\varepsilon}$ is unity but for a general medium it can be written as:

$$\hat{\varepsilon} = \begin{pmatrix} \tilde{\varepsilon}_{11} & \tilde{\varepsilon}_{12} & \tilde{\varepsilon}_{13} \\ \tilde{\varepsilon}_{21} & \tilde{\varepsilon}_{22} & \tilde{\varepsilon}_{23} \\ \tilde{\varepsilon}_{31} & \tilde{\varepsilon}_{32} & \tilde{\varepsilon}_{33} \end{pmatrix} \tag{2.10}$$

Each of the complex components $\tilde{\varepsilon}_{ij}$ is dimensionless and in general a frequency dependent function. Due to energy arguments it can be shown that

the dielectric tensor is symmetric, i.e. $\tilde{\varepsilon}_{ij} = \tilde{\varepsilon}_{ji}$. Every symmetric tensor is diagonalizeable by selecting a proper coordinate system. Thus, three complex functions describe the optical properties of each material:

$$\hat{\varepsilon} = \begin{pmatrix} \tilde{\varepsilon}_{11} & 0 & 0 \\ 0 & \tilde{\varepsilon}_{22} & 0 \\ 0 & 0 & \tilde{\varepsilon}_{33} \end{pmatrix} \tag{2.11}$$

For the general case of three different $\tilde{\varepsilon}_{ii}$ the medium is called anisotropic or biaxial. If two of the components are equal the material is termed uniaxial. Only for the isotropic case the tensor is reduced to a simple scalar function

$$\tilde{\varepsilon} = \varepsilon_1 + i\varepsilon_2, \tag{2.12}$$

where ε_1 and ε_2 are the real and imaginary part of the complex dielectric function. The optical properties of a medium can also be described by using the complex index of refraction

$$\tilde{n} = n + ik \tag{2.13}$$

Both equivalent representations can be transferred into each other using the following relations:

$$\varepsilon_1 = n^2 - k^2 \tag{2.14}$$

$$\varepsilon_2 = 2nk \tag{2.15}$$

and

$$n = \sqrt{\frac{1}{2}\left(\sqrt{\varepsilon_1{}^2 + \varepsilon_2{}^2} + \varepsilon_1\right)} \tag{2.16}$$

$$k = \sqrt{\frac{1}{2}\left(\sqrt{\varepsilon_1{}^2 + \varepsilon_2{}^2} - \varepsilon_1\right)}. \tag{2.17}$$

The electromagnetic absorption α of a medium can be calculated directly from the imaginary part of the complex index of refraction by

$$\alpha = \frac{4\pi k}{\lambda}. \tag{2.18}$$
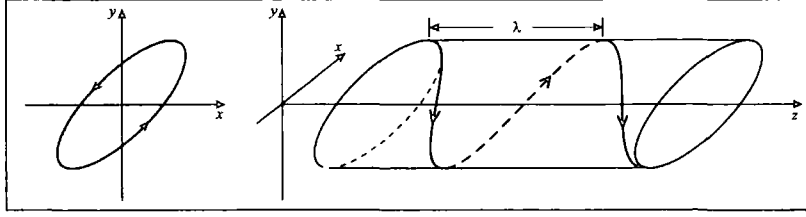
Fig. 2.1: Rotation of the electric field vector in the x-y plane and the trajectory of the electric field at a time t (adapted from [7])

2.1.2 Polarization States

The Polarization Ellipse

To describe the polarization state of an electromagnetic wave, only direction and phase of the E-field vector is required. For a wave propagating in the z direction and the field vector oscillating in the x-y plane the electric field components can be expressed as:

$$E_x = a_x \exp\left[2\pi\nu\left(t - \frac{z}{c}\right) + i\delta_x\right] \qquad (2.19)$$

$$E_y = a_y \exp\left[2\pi\nu\left(t - \frac{z}{c}\right) + i\delta_y\right]. \qquad (2.20)$$

By replacing the phase difference $\delta_y - \delta_x$ with Δ, these equations can be written as

$$\frac{E_x^2}{a_x^2} + \frac{E_y^2}{a_y^2} - 2\cos\Delta\,\frac{E_x E_y}{a_x a_y} = \sin^2\Delta \qquad (2.21)$$

which represents the parametrical description of an ellipse with the major and minor axis a_x and a_y and the phase difference of Δ. This is the most general case of the polarization of a planar wave and is called elliptical polarization (Fig.2.1). The two components of the electric field can also be expressed as an vector:

$$\vec{E} = \begin{pmatrix} \tilde{E}_p \\ \tilde{E}_s \end{pmatrix} = \begin{pmatrix} E_p \exp(i\delta_p) \\ E_s \exp(i\delta_s) \end{pmatrix} \qquad (2.22)$$
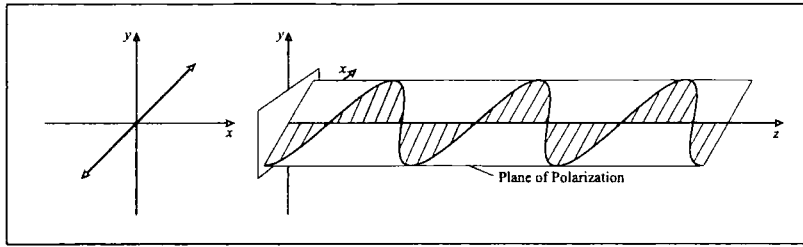
Fig. 2.2: Linearly polarized light oscillating in the x-y plane and the trajectory in the plane of polarization at a time t (adapted from [7])

The p- and s-notation of the light components in this Jones vector representation are symbolic for parallel and senkrecht (German for perpendicular) to the plane of incidence at interactions with a surface. Every interaction of the light beam can therefore be described by means of a 2×2 transfer matrix, known as the Jones Matrix.

Linearly Polarized Light

Light is called linearly polarized if one of the axes of the ellipse vanishes, e.g. $a_x = 0$, or if the phase difference of the components is zero or π. The general elliptical cylinder in Fig.2.1 is then compressed to a plane. The wave is therefore said to have planar polarization (Fig.2.2). The Jones vector representation of linearly polarized light is

$$\vec{E} = \begin{pmatrix} E_p \exp(i\delta) \\ E_s \exp(i\delta) \end{pmatrix} \tag{2.23}$$

The normalized Jones vector for p- and s-polarized light can be written as

$$\vec{E_p} = \begin{pmatrix} 1 \\ 0 \end{pmatrix} \quad \vec{E_s} = \begin{pmatrix} 0 \\ 1 \end{pmatrix} \tag{2.24}$$
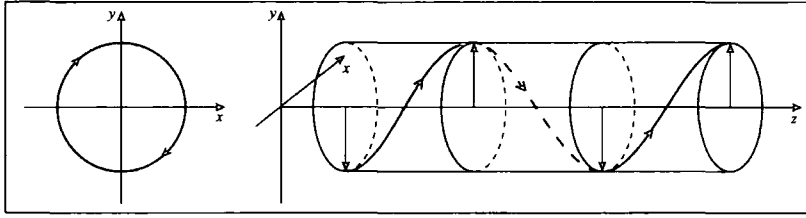
Fig. 2.3: Electric field vector circulating in the x-y plane and the trajectory of the electric field at a time t of circularly polarized light (adapted from [7])

Circularly Polarized Light

If the phase difference between $\vec{E}_x$ and $\vec{E}_y$ is $\Delta = \pm\pi/2$ and $a_x = a_y$ the polarization is called circular. The general elliptical cylinder in Fig.2.1 transforms into a circular cylinder (Fig.2.3). For the case of $\Delta = +\pi/2$ the resulting electric field vector rotates clockwise in the x-y plane and the polarization is called right circularly. For $\Delta = -\pi/2$ the counterclockwise rotating field vector defines the left circularly polarized light shown in Fig.2.3.

2.2   Ellipsometry

2.2.1   Light Reflection from a Planar Surface

To describe the reflection of a wave on the planar boundary between two optical systems it is sufficing to know the solution for any two mutually perpendicular polarizations. Normally, the directions perpendicular and parallel to the plane of incidence (s and p polarized light Fig.2.4) are used. In the Jones vector representation the reflected light beam can be described by

$$\begin{pmatrix} \tilde{E}_p^r \\ \tilde{E}_s^r \end{pmatrix} = \begin{pmatrix} \tilde{R}_{pp} & \tilde{R}_{sp} \\ \tilde{R}_{ps} & \tilde{R}_{ss} \end{pmatrix} \begin{pmatrix} \tilde{E}_p^i \\ \tilde{E}_s^i \end{pmatrix} \tag{2.25}$$
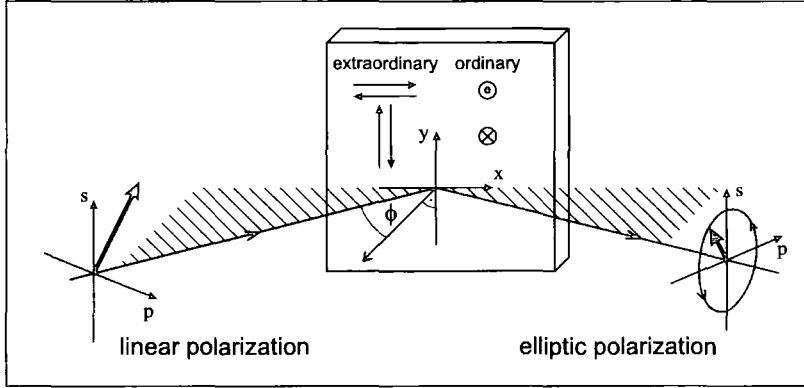
Fig. 2.4: Change in polarization of reflected light. Ordinary and extraordinary direction and s and p direction are shown

In the most general case all matrix elements are non-zero. The off-diagonal elements mix s and p-polarized light and mode coupling occurs. Only for isotropic and special cases of anisotropic optical functions the transformation matrix is diagonal.

$$
\begin{pmatrix} \tilde{E}_p^r \\ \tilde{E}_s^r \end{pmatrix} = \begin{pmatrix} \tilde{R}_p & 0 \\ 0 & \tilde{R}_s \end{pmatrix} \begin{pmatrix} \tilde{E}_p^i \\ \tilde{E}_s^i \end{pmatrix} \tag{2.26}
$$

Thus s and p-polarized light can change in amplitude but is not affected in its polarization state. The s and p polarizations are eigenvectors of the transformation matrix. For the diagonal elements it follows:

$$
\tilde{R}_{p,s} = \frac{\tilde{E}_{p,s}^r}{\tilde{E}_{p,s}^i} \tag{2.27}
$$

For an isotropic medium $\tilde{R}_p = \tilde{R}_s$. If the reflection coefficients are not equal but the transformation matrix diagonal, the optical response is called uniaxial. The complex index of refraction in the direction of the surface normal in such a material is different to the index parallel to the surface. Because of this relation between the coordinate systems of surface and optical system the transformation matrix becomes diagonal.

All the above considerations can also be made for the transmission coefficients of this interaction with a plane surface. The matrix elements are then replaced by $\tilde{T}_p$ and $\tilde{T}_s$. For the connection between the optical functions of the material and the reflection/transmission coefficient information about the angle of the reflected and refracted beam are necessary. By using Maxwell's equations (2.1..2.4) and the equality of phase at the interface, Shell's law can be calculated [6]:

$$\tilde{n}_0 \sin \phi_0 = \tilde{n}_1 \sin \phi_1, \qquad (2.28)$$

where ϕ_0 is the angle of incidence, measured between the surface normal and the light beam, and ϕ_1 the angle of the refracted beam in the second medium. The angle of the reflected beam is equal to the angle of incidence. The wave equations for all three beams can be written as

$$\vec{E}_{p,s}^i(\vec{r},t) = \tilde{E}_{0p,s}^i \exp\left(-i\,\vec{q_0}^i \cdot \vec{r}\right) \exp(-i\omega t) \qquad (2.29)$$

$$\vec{E}_{p,s}^r(\vec{r},t) = \tilde{E}_{0p,s}^r \exp\left(-i\,\vec{q_0}^r \cdot \vec{r}\right) \exp(-i\omega t) \qquad (2.30)$$

$$\vec{E}_{p,s}^t(\vec{r},t) = \tilde{E}_{0p,s}^t \exp\left(-i\,\vec{q_1}^t \cdot \vec{r}\right) \exp(-i\omega t) \qquad (2.31)$$

whereby the optical function and the angle is included in the wave vector $\vec{q} = -\frac{2\pi}{\lambda}\tilde{n}\vec{e}$ with $\vec{e}$ a unity vector in the direction of propagation of the wave. The calculation of Eq.2.27 from the wave equations yields an expressions for the reflection and transmission coefficients in terms of $\tilde{n}$ and ϕ:

$$\tilde{R}_p = \frac{\tilde{n}_1 \cos \phi_0 - \tilde{n}_0 \cos \phi_1}{\tilde{n}_1 \cos \phi_0 + \tilde{n}_0 \cos \phi_1} \qquad (2.32)$$

$$\tilde{R}_s = \frac{\tilde{n}_0 \cos \phi_0 - \tilde{n}_1 \cos \phi_1}{\tilde{n}_0 \cos \phi_0 + \tilde{n}_1 \cos \phi_1} \qquad (2.33)$$

$$\tilde{T}_p = \frac{2\tilde{n}_0 \cos \phi_0}{\tilde{n}_1 \cos \phi_0 + \tilde{n}_0 \cos \phi_1} \qquad (2.34)$$

$$\tilde{T}_s = \frac{2\tilde{n}_0 \cos \phi_0}{\tilde{n}_0 \cos \phi_0 + \tilde{n}_1 \cos \phi_1} \qquad (2.35)$$

2.2.2 Basic Concept of Ellipsometry

By dividing the two orthogonal field components in the s and p directions of an electromagnetic wave (Eq.2.19 and 2.20)

$$\frac{E_p}{E_s} = \frac{a_p}{a_s} \exp\left(i[\delta_p - \delta_s]\right) \tag{2.36}$$

an expression is obtained, which includes all necessary parameters to describe the state of polarization. These ellipsometric parameters are usually quoted as Δ and Ψ:

$$\Delta = \delta_p - \delta_s \quad \text{and} \quad \Psi = \arctan\left(\frac{a_p}{a_s}.\right) \tag{2.37}$$

All methods measuring these parameters belong to ellipsometry.

To obtain the change in polarization by interaction at the interface of a medium the ratio between the reflectivity of p and s polarized light is to analyze:

$$\frac{\tilde{R}_p}{\tilde{R}_s} = \frac{\frac{a_p^r}{a_p^i} \exp\left(i[\delta_p^r - \delta_p^i]\right)}{\frac{a_s^r}{a_s^i} \exp\left(i[\delta_s^r - \delta_s^i]\right)} = \tan\Psi \exp(i\Delta). \tag{2.38}$$

Generally Δ is the change in the phase difference and Ψ the magnitude of the ratio of the reflection coefficients in the p and s direction. By setting Eq.2.32 and Eq.2.33 in this last expression the measured ellipsometric parameters can be related to the optical functions.

2.2.3 Optical Components

Light Source

The optimal light source for ellipsometry would exhibit a stable output with high intensity over a large spectral range. The usually used Xe and Hg-Xe arc lamp fulfil this demand in a reasonable way. However, very high intensity at various atomic emission lines has to kept in mind when using this kind
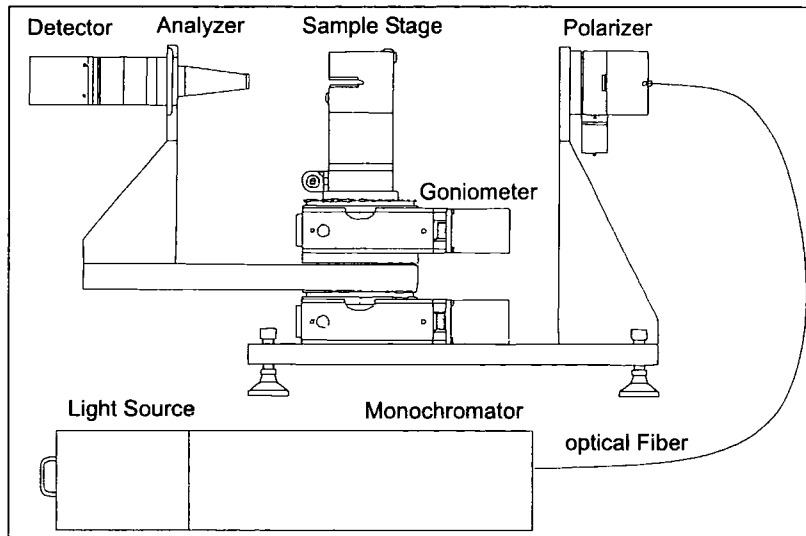
Fig. 2.5: Typical setup of an variable angle spectroscopic ellipsometer with its optical components (Woollam V-VASE Ellipsometer adapted from [8])

of light source. For wavelength dependent measurements, these light sources are spectrally dispersed using a monochromator.

Polarizer

To create a well defined linear polarization of the unpolarized light from the Xe arc lamp a polarizer is used. Unpolarized light consists of a variety of randomly polarized electric field vectors. Only the part of these vectors in the direction of the transmission axis of the polarizer will not be absorbed and the light beam becomes linearly polarized. High quality polarizer commercially available exhibit a polarization value of 10^6, i.e. it is linearly polarized to 1 part in 10^6. By rotating the polarizer along its azimuth angle linearly polarized light with a different ratio of s and p polarization can be obtained. Well defined elliptical polarization can be achieved if an retarder is inserted into the light beam after the polarizer. This element introduces a phase

delay between perpendicular light polarizations and is usually constructed from thin birefringent plates.

Analyzer

The Analyzer is usually identical to the polarizer and blocks all polarization directions except the one in the variable transmission axis. This is used to analyze every direction of polarization separately in order to determine the full polarization state of the light beam after the interaction with the sample.

Detector

The ideal detector for ellipsometry exhibit a polarization and wavelength independent sensitivity with a linear respond to the incident beam intensity. For a broad spectral range this is given by semiconductor photodiode detectors of Si or InGaAs. Alternatively, photomultiplier tubes can be used for detection but require accurate adjustment.

2.2.4   Ellipsometer Types

A short summary about commonly used ellipsometer types [8] is given in this section. All ellipsometers are able to measure in a wide spectral range but also at only one single wavelength.

Null Ellipsometry

The configuration of a null ellipsometer is as follows:

Source $\Rightarrow$ Polarizer $\Rightarrow$ Compensator $\Rightarrow$ Sample $\Rightarrow$ Analyzer $\Rightarrow$ Detector

The orientation of polarizer, compensator and analyzer is adjusted to give a 'null' respond in the detector for the measurement. This slow but accurate measurement is usually performed manually.

Polarization Modulation Ellipsometer

The configuration of a polarization modulation ellipsometer is as follows:

Source ⇒ Polarizer ⇒ Modulator ⇒ Sample ⇒ Analyzer ⇒ Detector

The modulator is hereby a time dependent retarder running at high speed. The high data acquisition rate of this method requires a very intensive light source (laser) or longer iteration times for a reasonable signal to noise ratio. Complicated calibration and high sensitivity to ambient temperature makes this a difficult technique.

Rotating Element Ellipsometer

The configuration of a rotating element ellipsometer is as follows:

Source ⇒ Rotating Polarizer ⇒ Sample ⇒ Analyzer ⇒ Detector

or

Source ⇒ Polarizer ⇒ Sample ⇒ Rotating Analyzer ⇒ Detector

No retarding element is included in this configuration and the imperfect optical properties of compensators are removed. The disadvantage of such a ellipsometer is the loss of sensitivity if Δ is close to 0° or 180°, the indistinguishability of left and right circularly polarized light and the limitation in measurement speed by the rotation speed of the polarizer or analyzer.

Rotating Analyzer With Variable Retarder Ellipsometer

To improve the rotating analyzer ellipsometer a variable retarder after the polarizer and before the sample can be included. By adjusting the input polarization in this way the reflected light beam can always be close to a circular polarization and the measurement for Δ is accurately in the full range of 0° − 360°. This configuration is the most common type for high precession measurements at the moment.

Variable And Fixed Angle Ellipsometers

The most sensitive region of an ellipsometer is at the pseudo Brewster angle which results in Δ values around $90°$. This angle is dependent of the investigated material and only a variable angle ellipsometer is capable of taking measurements at multiple positions and at least one of the measured angles should be close to the pseudo Brewster angle.

By changing the angle of incident, the path length of the probe beam travelling through the film also can be changed which yields an increase of the information available for the analysis process.

2.2.5   Ellipsometric Parameters from Measured Data

The measured data from the rotating analyzer type ellipsometer is the time-dependent intensity of the light at the detector

$$I(t) = I_0 \left(1 + \alpha \cos[2A] + \beta \sin[2A]\right), \tag{2.39}$$

with α and β the normalized Fourier coefficients of the detector signal and A the azimuth angle of the analyzer. For the position of the analyzer holds:

$$A(t) = 2\pi f_0 t + \theta \tag{2.40}$$

For the general case of an anisotropic medium the Fourier coefficients are related to the reflection coefficients and polarizer azimuth P in the following way [8]:

$$\alpha = \frac{|\tilde{\rho}_{pp} + \tilde{\rho}_{sp}\tan P|^2 - |\tilde{\rho}_{pp}\tilde{\rho}_{ps} + \tan P|^2}{|\tilde{\rho}_{pp} + \tilde{\rho}_{sp}\tan P|^2 + |\tilde{\rho}_{pp}\tilde{\rho}_{ps} + \tan P|^2} \tag{2.41}$$

$$\beta = \frac{2\,\Re\left\{(\tilde{\rho}_{pp} + \tilde{\rho}_{sp}\tan P)(\tilde{\rho}_{pp}\tilde{\rho}_{ps} + \tan P)\right\}}{|\tilde{\rho}_{pp} + \tilde{\rho}_{sp}\tan P|^2 + |\tilde{\rho}_{pp}\tilde{\rho}_{ps} + \tan P|^2}. \tag{2.42}$$

The normalized reflection matrix elements are defined by:

$$\tilde{\rho}_{pp} = \frac{\tilde{R}_{pp}}{\tilde{R}_{ss}} \qquad \tilde{\rho}_{ps} = \frac{\tilde{R}_{ps}}{\tilde{R}_{pp}} \qquad \tilde{\rho}_{sp} = \frac{\tilde{R}_{sp}}{\tilde{R}_{ss}}. \tag{2.43}$$

Are the Fourier coefficients determined during the measurement, the reflection matrix can be calculated by a regression process [9] using Eq.2.41 and 2.42.

For the simple case of an isotropic material ($\tilde{\rho}_{ps} = \tilde{\rho}_{sp} = 0$) the ellipsometric parameters can be expressed directly in terms of polarizer angle and Fourier coefficients:

$$\tan \Psi = \sqrt{\frac{1 + \alpha}{1 - \alpha}} |\tan P| \tag{2.44}$$

$$\cos \Delta = \frac{\beta}{\sqrt{1 - \alpha^2}} \frac{\tan P}{|\tan P|}. \tag{2.45}$$

2.2.6 Regression Analysis of Optical Data

The measured parameters in ellipsometry are not the optical constants of the material. The relation of the ellipsometric parameters and the complex index of refraction is specified in Eq.2.38 together with Eq.2.32 and 2.33. However, there is no direct way to calculate n and k only by generating a model for the optical function of the system, the ellipsometric parameters can be determined.

The measured system is described by a model, which is used to simulate the experiment and to compare the results of this simulation to the experimental data. If the difference of both sets of data is very low, the optical function of the model should correspond to the function of the actual sample. Otherwise the model has to be varied and the influence of this change to be investigated. A flowchart of the data analysis procedure is shown in Fig.2.6
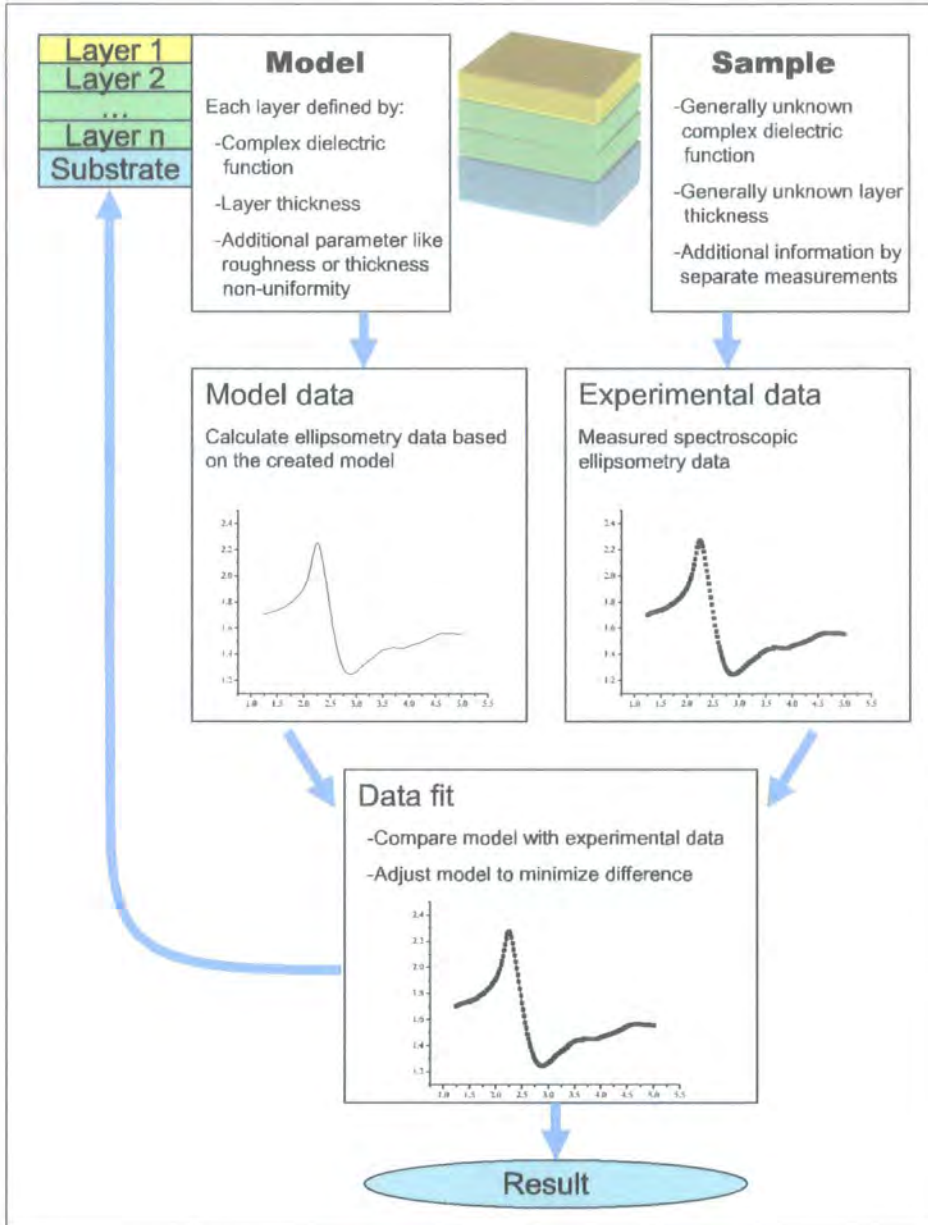
Fig. 2.6: Flowchart of the spectroscopic data analysis procedure

Maximum Likelihood Estimator

To compare simulated and experimental data, a way to evaluate the fit quality is necessary. This maximum likelihood estimator should give a positive value with a minimum for an exact match. The mean-squared error (MSE) is such a function:

$$MSE = \frac{1}{2N - M} \sum_{i=1}^{N} \left[\left(\frac{\Psi_i^{mod} - \Psi_i^{exp}}{\sigma_{\Psi,j}^{exp}} \right)^2 + \left(\frac{\Delta_i^{mod} - \Delta_i^{exp}}{\sigma_{\Psi,j}^{exp}} \right)^2 \right] = \frac{1}{2N - M} \chi^2$$

(2.46)

The number of (Ψ, Δ) pairs is N, M the number of variable parameter in the fitting process and σ the standard derivation of the experimental data points. The value of chi-squared, as defined in Eq.2.46, is also a commonly used maximum likelihood estimator.

Minimization of the MSE

To obtain the best possible fit for the simulated data, the model parameter values, which give a minimum MSE, have to be found. A simple method to analyze the change in the MSE due to a change in the parameters is the gradient method:

$$\delta a_k = c \frac{\partial \chi^2}{\partial a_k},$$

(2.47)

where a_k are the variable parameters in the model. The adjustment vector $\delta \vec{a}$ follows by taking the gradient of chi-squared times a chosen constant c. For steep gradients, bigger changes are made compared to a flat gradient around the minimum where only slight variations are better.

For the assumption of MSE being a quadratic function of the parameters close to the minimum the inverse Hessian method is a faster way to determine the settings for a minimum of chi-squared:

$$\vec{a}_{min} = \vec{a}_{current} + \vec{D}^{-1} \cdot \left[-\nabla \chi^2 (\vec{a}_{current}) \right].$$

(2.48)
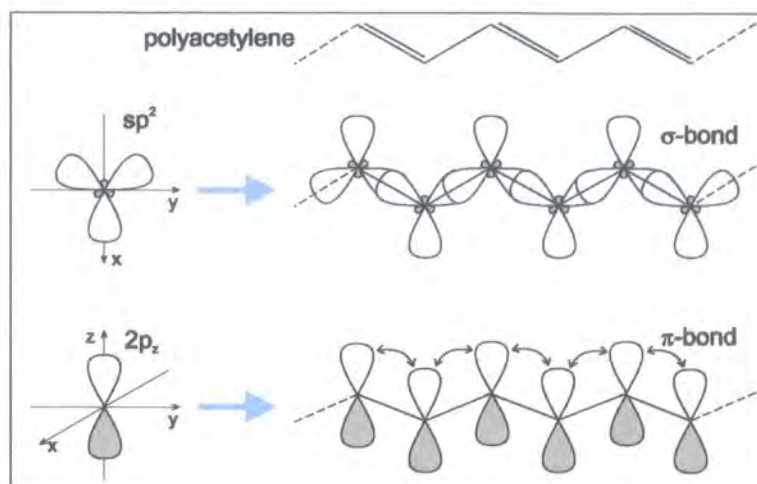
Fig. 2.7: Illustration of the sp^2 hybrids and the p_z orbital. The resulting σ-bonds and π-bonds for polyacetylene are shown (adapted from [10]).

In this expression $\vec{D}$ is an $M \times M$ matrix with the components $\partial^2 \chi^2 / \partial a_k \partial a_l$. By introducing the Marquardt parameter λ, which is multiplied to $\vec{D}^{-1}$ in the form $(\lambda + 1)$, a blending between the simple gradient method and the inverse Hessian algorithm can be carried out. This strategy is known as the Levenberg-Marquandt algorithm. For very small values of λ close to zero the inverse Hessian method and for large values of λ the gradient method are approximated.

2.3 Conjugated Polymers

2.3.1 Introduction in Conjugated Polymers

Polymers are long chains of atoms with repeating monomer groups. Organic polymers have stable chain structures because of the bonding properties of carbon. This group IV element has four valence electrons, two in the $2s$ and two in the $2p$ orbitals. These electrons can be hybridised and form sp^3

sp^2 or sp configurations. In organic polymers, sp^2 hybridised carbon atoms form strong localized sigma bonds with neighboring atoms. This structure represents the backbone of the polymer chain. The additional p_z orbital per carbon atom in conjugated polymers is perpendicular to the plane of sp^2 hybrid orbitals and contains one unpaired electron. The orbital configuration for the most simple conjugated polymer polyacetylene is shown in Fig.2.7. For this unsaturated carbon linkage a symmetrical combination of adjacent unpaired electrons in the p_z orbital results in the formation of a bonding π orbital or a anti-symmetrical combination in a antibonding π^* orbital. These π or π^* orbitals can overlap with the neighboring one and form a delocalized wavefunction spreading along many monomer units. The number of overlapping electron orbitals defines the conjugation length. In typical polymer systems this length is around ten repeat units [11]. Limitations in the conjugation length are due to twists in the chain and chemical impurities [12, 13].

2.3.2 Polymer Structure

The constitution of a polymer is affected by type, number and sequence of the monomer units, endgroups and linkages. Some major parameters to describe the polymer structure are given in this section.

Chain Length

The important polymer property of chain length is connected to the molar mass, the 'weight' of a molecule. Due to random changes in the synthesis process an exact number can not be given. The best way to characterize the polymer is in form of the distribution function for the molar mass. This function can be described by a variety of averages like *number average* $<M>_n$,

or *weight average* $<M>_w$. With N_i as the number of monomer units of type i and the molar mass M_i, these averages are defined by [14]

$$<M>_n \;=\; \frac{\sum N_i M_i}{\sum N_i} \tag{2.49}$$

$$<M>_w \;=\; \frac{\sum N_i M_i^2}{\sum N_i M_i}. \tag{2.50}$$

An alternative method to describe the chain length of polymers is the ratio between the appropriate average molar mass M and the molar mass of the monomer unit M_0 and is called average degree of polymerization x:

$$x = \frac{M}{M_0}. \tag{2.51}$$

Depending on the average molar mass used, the subscripts x_n and x_w are distinguished.

Polymer Size And Shape

The shape of a polymer molecule is not only determined by the chain length. The strength of the chemical linkage between the carbon atoms along the chain has influence on the stiffness of the polymer and the formation of the monomer units can decide whether the polymer is a one dimensional molecule or a more complex object.

To explain the different conformations, butane is used as an example. In this molecule the two methyl groups attached to neighboring carbon atoms are in general twisted to each other. The most stable conformation is a *dihedral angle* of $\phi = 180°$, which is called the *trans* position. This order represents the maximum distance for the methyl groups. Other formations are less stable but can also represent an energy minimum (*gauche* position). The two positions are depicted in Fig.2.8. This concept of *trans* and *gauche* connections is applicable on many polymers e.g. polyethylene. The monomer
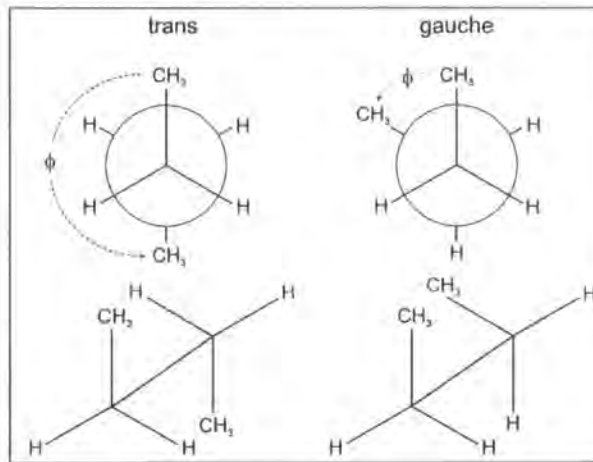
Fig. 2.8: Trans and gauche position of the butane molecule (adapted from [14])

units of this polymer consists of two carbon atoms which are connected with a bond angle θ that causes the molecule to be a zig-zag chain, comparable to Fig.2.7. This conformation represents the all *trans* configuration. A *gauche* position in the polymer rotates the chain out of its plane and a three dimensional molecule shape is obtained (Fig.2.9). In a realistic distribution of *trans* and *gauche* positions, for many polymer types a more coiled formation of the molecule is expected depending on the energy difference ΔE between the two positions. The temperature dependent relation of the number of *trans* and *gauche* states, n_t and n_g, is given by

$$\frac{n_g}{n_t} = 2 \exp\left(\frac{-\Delta E}{k_B T}\right) \tag{2.52}$$

with k_B as the *Bolzman* constant. Typical values at room temperature are around 0.5 (e.g. polyethylene).

However, the energy difference for conjugated polymers is much higher due to the additional π orbitals perpendicular to the main chain. These bonds form a support for the molecule and give it the typical rigid-rod character of conjugated polymers. These molecules exhibit no sharp bending on local
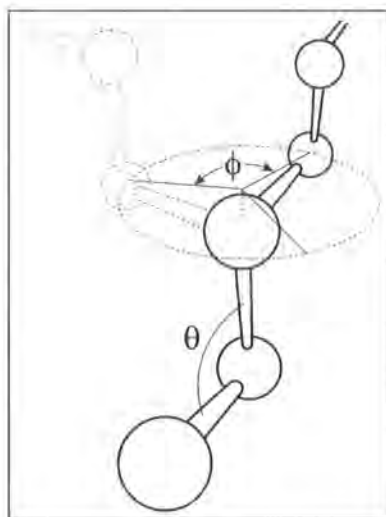
Fig. 2.9: All *trans* polyethylene molecule with bind angle θ (solid line) and molecule chain with one gauche rotation of angle ϕ (dashed line)

scales and the strength of the σ and π bonds affects the shape of the molecule. Very strong bonds causes a linear polymer chain but for weaker linkages a coiled conformation is also possible. Because of the origin of this property, the effect is called π-*stiffness*.

2.3.3   Excitation Theory in Conjugated Polymers

In non-conjugated polymers, only strong σ bonds between the carbon atoms and perhaps isolated π bonds are present. The large energy band gap E_g between these σ bonds and their antibonding σ^* counterparts make them electrical insulators and optically transparent. If in conjugated polymers all π and π^* electron orbitals would be delocalized, a half filled band of allowed states would exist via Pauli's principal. This band has no gap and the polymer could therefore be considered as a metal. However, this configuration is unstable to the Peierls transition [15]. The hereby opened up band gap lowers the total energy of the electrons in the system. If the energy needed

for this distortion of the bonds is below the electron energy reduction by this process, Peierls transition happens. Bond dimerization that results in short double bonds actually occurs in conjugated polymers and therefore they are intrinsically semiconductors. Furthermore, kinks and chemical impurities in this system reduce the delocalization of excited states and the conjugation of neighboring orbitals is limited to only a few repeat units instead of a delocalization along the whole chain.

Therefore, a correlation between the electron in the excited π^* orbital and the corresponding hole, due to coulomb attraction at a close distance, is present and this electron-hole pair is called exciton. The binding energy of such an exciton is the important factor, that determines the semiconductor properties of conjugated polymers.

Photoexcitation in this materials is to understand as an exciton formation introduced by the energy of the incident photon, i.e. the electron is excited from the π orbital into the antibonding π^* orbital and is still connected to the remaining hole. The exciton is initially promoted to higher vibronic states and will thermalize into the vibrational ground state from where it either recombines (radiative or non-radiative) or dissociates into a free charge carrier.

2.3.4 Optical Absorption in Conjugated Polymers

Initially, the ground state of the π orbital in conjugated polymer is occupied by electrons with opposing spins (singlet state). The wave function of the first exited state of the electron overlaps in general with the wave function of the ground state. For this reason a transition between these states is possible and the strength is dependent on the amount of overlap. The transition dipole moment μ_{fi} of this process (initial to final state) can be written as an

integration of the wave functions over their overlapping region together with μ, the dipole moment of this system [16]:

$$\mu_{fi} = \int \psi_f^* \mu \psi_i d\tau. \tag{2.53}$$

Because of the delocalization of the π orbital electrons along the chain in conjugated polymers, the direction of the dipole vector is highly oriented along the chain and $\pi - \pi^*$ transitions in this structure have a highly anisotropic character. Electromagnetic waves with an energy corresponding to the energy difference between these electronic states can therefore only be absorbed by the electron and the energy used for the transition, if the dipole vector of the wave matches, at least partially, the direction of the polymer dipole vector.

Optical transitions at multiple wavelengths are investigated by absorption spectroscopy. The strength of the transition between two energy states determines the ratio of incident light I_0 and the light emerging from a sample with thickness l, I_l. The *Beer-Lambert Law* expresses this ratio:

$$\frac{I_l}{I_0} = e^{-\alpha l}. \tag{2.54}$$

The absorption coefficient α is connected to the transition dipole moment by [16]

$$\int \alpha d\nu = \frac{\pi \nu_{fi}}{3\varepsilon_0 \hbar c} L |\mu_{fi}|^2 \tag{2.55}$$

with L the orbital angular momentum and ν_{fi} the frequency of the transition.

2.4   Organic Optoelectronic Devices

2.4.1   Introduction

Conjugated polymers have a growing importance for the usage in optoelectronic devices due to their semiconductor properties. The main reason for the usability in such devices is the location of the band gap energy in the range of visible light. Thus, photovoltaic and light emitting devices are the first applications of this material group. The advantage of using conjugated polymers rather then anorganic semiconductors is the simplicity of fabrication and thus low-cost manufacturing. The lower brightness and shorter lifetime of organic devices compared to the anorganic counterparts are still limiting factors for potential fields of application.

2.4.2   PLED Structure

In the most simple case, a polymer light emitting diode (PLED) is constructed from just three layers [17], a thin conjugated polymer film sandwiched between two electrodes. For one electrode a low work function metal is used as an electron injector and for the other one a high work function metal as a hole injector. The work function of the electrode describes the energy needed to bring one electron out of the material into vacuum at infinite distance. This value should match the energy level of the polymer as close as possible. Under sufficient forward bias the electrons and holes injected in the conduction and valence band respectively can capture one another within the polymer film and form excitons. This excited state is able to decay by emitting a photon. The electric field, as the cause of the light emission in the device, determines the notation of the effect as electroluminescence. A schematic band diagram for a PLED is depicted in Fig.2.10.
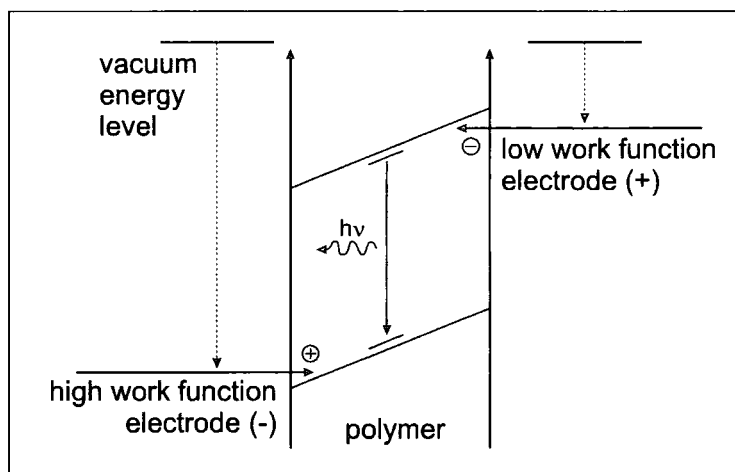
Fig. 2.10: Schematic band diagram for PLED under forward bias

Common metals for the electrodes are Indium Tin Oxide (ITO) with the high work function of 4.7 eV and Calcium as an electron injector with a work function of 2.3 eV. Better results for actual applications such as improved efficiency are obtained by using a second conjugated polymer, like PEDOT-PSS [18], as high work function buffer layer at the ITO electrode. For this material the injection barrier as the difference between electrode work function and polymer energy level can be decreased and the injection probability be increased.

Another factor that limits the efficiency of PLEDs is the number of charge carrier traps in the polymer film that prevent the injected electrons and holes from recombination. Furthermore not all generated photons can leave the device and contribute to the external light output due to absorption in the device and total internal reflection at boundary layers. The external quantum efficiency (EQE) η_{ext} gives the ratio of applied electric energy and the actual energy output from the device in form of photons and includes all losses in the PLED.

Chapter 3

Experimental Techniques

3.1 Sample Preparation

In this study, thin films of the conjugated polymers $poly(2 - methoxy, 5 - (2' - ethyl - hexyloxy) - p - phenylenevinylene)$ (MEH-PPV), $poly(2, 5 - pyridinediyl)$ (PPy) and the PFO derivative $\alpha, \omega - Bis[N, N - di(5 - methyl\ phenyl)aminophenyl] - poly(9, 9 - bis(2 - ethylhexyl)fluoren - 2, 7 - diyl)$ (PF2/6am5) are investigated. Two different sample structures were used for optical measurements (Fig.3.1). Silicon wafers are well suited substrates for ellipsometry measurements because of their high reflectivity and nearly perfect mirror property. The wafers used exhibit a variable thickness of their SiO_2 layer between native oxide of 2 nm and about 130 nm resulting from a thermally activated growing process. The thin polymer film was created by spin casting a polymer solution on top of this substrate. For transmission measurements, the silicon wafer was replaced by a disc of fused silica (quartz) in order to have no absorbtion from the substrate.
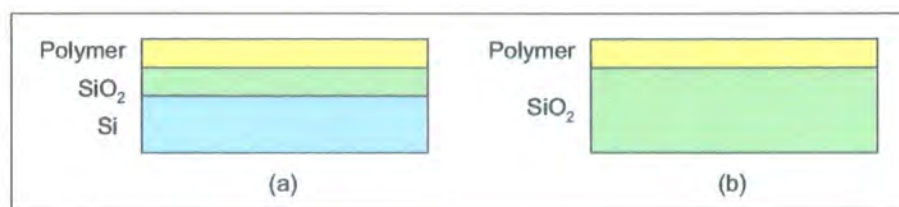
Fig. 3.1: Sample structure (a) for ellipsometric measurements (b) for transition measurements

Polymer	PPy	MEH-PPV	PFO
Solvent	formic acid	toluene	toluene
Concentration (mg/ml)	20	8	15
Film thickness (nm)	70	100	70

Table 3.1: Solution concentration and film thickness relation

Polymer Solution

To obtain a smooth and homogeneous polymer film, necessary for ellipsometric measurements, the choice of a matching solvent is very important. The solvents, used in this study, are toluene and chlorobenzene for MEH-PPV and the PFO derivatives, and formic acid was used for PPy. The concentration of the solution was chosen to give a polymer film thickness of about 100 nm. Typical relations between concentration and film thickness are listed in Table 3.1. There is no relevant difference between toluene and chlorobenzene in film quality and resulting thickness.

All solutions were prepared by stirring the polymer powder together with the solvent for a certain time dependent on the solubility of the specific polymer. PFO dissolves almost instantly but PPy and MEH-PPV need about 20 min or 60 min respectively but dependent of the concentration aspired.

Spin-Casting

To obtain a thin polymer film of about 100 nm with high thickness uniformity and a smooth surface, spin casting is the most common method. The polymer solution is thereby dropped onto the substrate and the sample then rotated at high speed. The usual setting in this work are 2500 rpm for 60 seconds. The values from Table 3.1 are obtained at these settings. To avoid any structural differences by varying the thickness of the polymer film all samples for on set of measurements were created under identical conditions.

Thickness Measurement

The analysis of the ellipsometry data yields the optical constants n and k as well as the thickness of the polymer layer. In order to check the value obtained for the thickness, a Tencor Alpha-Step thickness profiler was used. For this measurement a small part of the polymer film was removed from the substrate using a scalpel blade. The stylus of the profiler draws across the surface with the removed section and produces a profile of it. The thickness can be determined by taking the difference value between the polymer covered substrate and the blank one. Measuring only the polymer surface yields information about surface roughness. The lower limit in the accuracy of this method is about 5 nm and thus, only a rough approximation for the actual thickness can be given.

3.2 Optical Measurements

To obtain enough information for modelling the optical properties of the polymer films investigated, variable angle spectroscopic ellipsometry measurements (VASE) and intensity transmission measurements were carried

out. For each polymer at least four samples with a different thickness of the oxide layer on top of the silicon substrate were investigated by ellipsometry, and transmission data was acquired for one sample. For all optical measurements a J.A.Woolam Co. V-VASE instrument was used. The rotating analyzer type ellipsometer is described in section 2.2.4. The spectral range of the ellipsometer, in which reliable data can be acquired, covers energies between 0.73 and 5.00 eV. Because of the limited range for the optical fibers, a single measurement can not be made in the complete spectrum and two passes with different fibers at each time are necessary to obtain data for the full spectral range.

3.2.1 Intensity Transmission Measurements

Intensity transmission measurements were carried out at normal incidence (straight through position of the ellipsometer). Monochromatic linearly polarized light in the range of 1.24 to 5 eV was used. The polarization direction didn't affect the transmittance spectrum and polarized light was used because of no option for unpolarized light in the ellipsometer settings. Only for samples with biaxial optical response, i.e. with in-plane anisotropy, the polarization direction would be noticeable in the data. The spectrum was acquired in steps of 20 meV and the detector signal typically averaged over 50 revolutions of the analyzer. To determine the transmittance spectrum of the polymer film, the detector signal without the sample in the light beam was recorded first. The detector values for the measurement with sample were divided by the values of the background data to obtain the actual transmittance. Since the detector signal will change after the recording of the background spectrum due to fluctuating lamp intensity and variable ambient light, the reliability of this type of measurement is not as high as for data

from specialized equipment. In order to minimize these influences, the ellipsometer was covered by a black paperboard box to avoid ambient light and the lamp was allowed to warm up for at least 20 min to minimize fluctuations.

3.2.2   Ellipsometric Measurements

The ellipsometric parameters Ψ and Δ were acquired in the spectral range between 1.24 and 5 eV in steps of 20 meV. The assumption of a uniaxial optical respond of the polymer film necessitate data at multiple angles of incidence. For an angle of 0° between surface normal and light beam only the complex index of refraction in the ordinary direction is probed. Not until an incident angle close to 90° is applied, a significant influence of the extraordinary part of the refractive index is observed. To determine the optical functions of conjugated polymers, at least one angle of incident should therefore be in this region. Values of 65°, 75° and 85° were used for the ellipsometric measurements in this work.

Because of a low signal intensity for light energy values between ca. 4.5 eV and 5.0 eV, a variable integration time of up to 200 analyzer revolutions is necessary for a high signal to noise ratio.

The ellipsometer used is equipped with an autoretarder input unit to keep track of the depolarization by the sample. Since surface roughness causes high depolarization of the reflected light beam, a statement about film quality was made by considering these values. Apart from this, mode coupling between the two polarization directions s and p during the surface interaction (see section 2.1.2) is also measurable with the aid of the autoretarder. Conversion of s into p polarized light and vise versa is only present for biaxial and some cases of uniaxial materials. For polymer films with isotropic and special cases of uniaxial optical response, no mode coupling is expected. Thus,

the measurement of these values gives information about the optical model required in the analysis process.

3.3 Non-linear Regression Analysis of Ellipsometry Data

Since ellipsometry doesn't measure the optical functions of a system but parameters that can be calculated from them, a numerical analysis is necessary to obtain the complex index of refraction. For the simulation of the ellipsometry experiment a model representing the measured structure was created. Information about the layer formation and an approximation of the optical function is required for this model (see section 2.2.6). For the fitting process WVASE32^{TM} software (v. 3.361) from J.A.Woolam Co. was used.

3.3.1 Layer Structure Modelling

At first the oxide layer thickness of the silicon wafer, used later as a substrate for the polymer films, was determined by ellipsometry prior to the spin casting. The model for the wafer consist of a 1 mm thick silicon substrate with a SiO_2 layer on top of it. Light is not able to penetrate very deeply into the silicon and the exact thickness is not crucial in the model. The thickness of the oxide layer was calculated using the regression process and compared to that expected from the oxide layer growth conditions. Optical constants for silicon and SiO_2 were taken from tabulated optical reference data [19].

For the spin cast polymer film on the silicon wafer, a special layer, simulating uniaxial optical response, was added in the sample model. Two independent optical functions for the ordinary and extraordinary direction are distin-

guished in this layer type. The parameterization of these functions is made in two separate zero thickness layers, which are linked to the uniaxial layer. The model for the transmission measurements only consists of a 1 mm fused silica layer (SiO_2) and the uniaxial layer described above. Since the quartz disc is expected to have no absorption in the measured spectrum, the SiO_2 substrate does not affect the analysis and is only present because a model with only one layer is not able to fit the thickness of this single layer.

3.3.2 Parameterization of Optical Functions

At first, a simple parametric model for the polymer was used in the regression process. An oscillator model was thereby applied to each of the optical functions in the ordinary and extraordinary direction. This oscillator model allows an approximation of the actual complex index of refraction by one or more different oscillator types. In this work, the following oscillators are used:

$$\text{Cauchy:} \quad n = A_n + \frac{B_n}{\lambda^2} + \frac{C_n}{\lambda^4} + ... \tag{3.1}$$

$$k = A_k \exp\left(B_k \cdot 1.24\left(\frac{1}{\lambda} - \frac{1}{C_k}\right)\right) \tag{3.2}$$

$$\text{Lorentz:} \quad \tilde{\varepsilon} = \frac{A_n \cdot Br_n \cdot E_n}{E_n^2 - E^2 - iBr_nE} \tag{3.3}$$

$$\text{Gaussian:} \quad \varepsilon_1 = \frac{2}{\pi}P\int_{R_g}^{\infty}\frac{\xi\varepsilon_2(\xi)}{\xi^2 - E^2}d\xi \tag{3.4}$$

$$\varepsilon_2 = A_n \exp\left(-\frac{E - E_n}{Br_n}\right) + A_n \exp\left(-\frac{E + E_n}{Br_n}\right). \tag{3.5}$$

The parameters with index n or k are fitting parameters, that will be optimized during the analysis process. Detailed information about the oscillator models can be found in the WVASE32^{TM} software manual [8].

With a Cauchy background and one Gaussian oscillator for each of the dielectric functions, a coarse approach to the real functions was initially found. Two main strategies are possible to improve this start value. To add more oscillators in order to increase the number of parameters for the modelling is one way for a more precise result. A good match of the simulated data to the experimental one was usually given by using a Cauchy background and about eight Gaussian oscillators for approximating each of the complex dielectric functions.

The second possibility is fitting n(E) for each wavelength separately (point-by-point fit) with the first approximation as the start value. This method is independent of any parametrical model for the functions and a high level of consistency to the experimental data is achievable. Since every n and k value at the different energies is a separate fitting parameter, the numerical effort is significantly higher then for a parametrical model. Because of the large number of independent values, the higher correlation between these fitting parameters has to be considered and start values as close as possible to the actual functions are vital for a confident result.

3.3.3 Advanced Fitting Techniques

The number of unknown parameter in the study of conjugated polymer films is to high to determine them only by a single ellipsometric measurement and every additional piece of information can be helpful for the analysis process. The acquiring of data at multiple angles of incidence is one of the possibilities. During the regression analysis all parameters are optimized to fit the data for each angle at the same time. In the same way, the comparison between simulated and experimental results can be made for not only one measured structure. By using the data of multiple samples with the same

uniaxial model for the polymer film in the fitting process simultaneously, the correlation between the model parameters was reduced. Since the preparation process of the polymer layer was identical for all samples, the application of the same optical functions $\tilde{n}_o = n_o + ik_o$ and $\tilde{n}_e = n_e + ik_e$ to each polymer film should be a realistic assumption. VASE data of up to nine, but usually four, samples and polarized transmission intensity data was used in this work for the multiple-sample non-linear regression analysis.

The layer model discussed above (see Fig.3.1) represents the most elementary assumption that yields useful results. Many simplifications such as perfectly smooth surfaces and sharp layer boundaries are made, which are unlikely to be present in the actual sample. These imperfections can also be simulated in the model by including additional parameters in it. Possibilities provided by the software are, e.g. surface roughness layer and effective medium approximation layer to simulate a soft change of optical constants between two layers. Furthermore thickness non-uniformity and errors in the experimental setup data such as angle of incidence, can be considered in the analysis. However, each of these additional parameters causes higher correlation and was only applied, if no satisfying fit was obtained by using the most simple model possible. For samples with well defined structure and high film quality, which was the usual case in this study, none of the extended parameters are necessary.

3.4 Internal Quantum Efficiency Calculation for PLEDs

A crucial property of a light emitting device is the external quantum efficiency (EQE η_{el}^{ext}). This value describes the relation between the applied electric
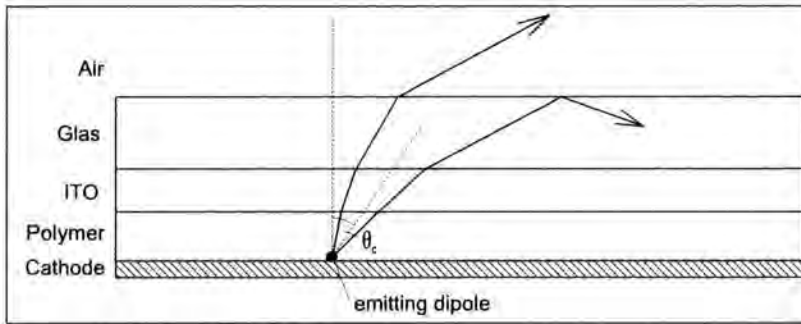
Fig. 3.2: Schematic diagram showing photon surface-emission in a simple PLED structure used for the "half-space" model

energy and the photon energy emitted from the PLED. To maximize this efficiency is an important goal in the investigation of conjugated polymers and their applications. But to understand internal effects in these materials, the internal quantum efficiency (IQE η_{el}^{int}) is more suitable to consider. This value represents the ratio between applied electric energy and internally generated photon energy. The calculation of this factor after the measurement of EQE is described in this section.

3.4.1 Half-Space Model

To calculate the IQE from the measurement of the EQE, a simple "half-space" optical model, developed in [20], was assumed for the PLED. Light is thereby generated from exciton recombination by dipoles in front of the metal-polymer interface and the cathode is expected to be a perfect mirror. Only light escaping directly through the surface is collected in the EQE measurements. The surface-emission zone is defined by the angular range of the escaping light: $0 \leq \theta_{em} \leq \theta_c$ (Fig.3.2). The critical angle θ_c is a function of the index of refraction and wavelength dependent:

$$\theta_c = \arcsin \frac{n_{air}}{n_{polymer}(\lambda)} \tag{3.6}$$

A 100% transmission is assumed for this area and any other light is lost for the external measurement through wave guiding and absorption. The out-coupling constant ξ for this model, which represents the ratio between external and internal quantum efficiency, can be calculated by dividing the light intensity integrated over the emission cone by the total hemispherical emission.

$$\xi = \frac{\eta_{el}^{ext}}{\eta_{el}^{int}} = \frac{\underset{\text{surface emission cone}}{\iint} I(\theta_{em})}{\underset{\text{hemisphere}}{\iint} I(\theta_{em})} \tag{3.7}$$

3.4.2 IQE of Isotropic Polymers without Dispersion

Since accurate information about the optical response of thin films of conjugated polymer was not available for recent studies, a simple wavelength independent isotropic index of refraction was usually assumed [21, 22]. This case allows the calculation of the critical angle for the surface emission directly from the constant index of refraction n_p:

$$\sin \theta_c = \frac{1}{n_p}. \tag{3.8}$$

The isotropic dipole distribution, present in this approximation, leads to a constant emission intensity over the emission angle:

$$I_{em}(\theta_c) = \text{const} = C. \tag{3.9}$$

Thus, the ratio of the integrals in Eq.3.7 for the calculation of the out-coupling efficiency expresses the ratio of the integration areas:

$$\xi = \frac{\int\limits_{2\pi}^{0} \int\limits_{\theta_c}^{0} CR^2 |\sin\theta| d\theta d\varphi}{\int\limits_{2\pi}^{0} \int\limits_{\frac{\pi}{2}}^{0} CR^2 |\sin\theta| d\theta d\varphi} = 1 - \cos\theta_c, \tag{3.10}$$

and using Eq.3.8 yields:

$$\xi = 1 - \cos(\arcsin\frac{1}{n_p}) = 1 - \sqrt{1 - \frac{1}{n_p}}. \tag{3.11}$$

The usual approximation for large n, that can be found in many publications, is:

$$\xi = 0.5n^{-2} \tag{3.12}$$

3.4.3 IQE of Devices with Anisotropic Active Layer

The complex index of refraction and the emission intensity is in general dependent on the direction in the polymer film because of the anisotropic nature of these films. The critical angle for the surface emission is thus not a simple function of a constant n_p value but an expression including the index of refraction in ordinary and extraordinary direction ($n_\perp$ and $n_\parallel$) as well as the critical angle itself:

$$\sin\theta_c = \sqrt{\frac{\cos^2\theta_c}{n_\perp^2} + \frac{\cos^2\theta_c}{n_\parallel^2}}. \tag{3.13}$$

From given data of the anisotropic index of refraction, the critical angle was determined by numerical analysis.

The anisotropic optical property in conjugated polymers is directly connected to the chain conformation and thus results in an angle dependent emission intensity since the emitting dipoles are along the polymer chain (section 2.3.2). For a uniaxial configuration, with the optical axis parallel to the surface normal, the angle dependency can be written as [23]:

$$I_{em}(\theta_{em}) \propto 1 + \cos^2\theta_{em}. \tag{3.14}$$

The integral equation 3.13 yields therefore:

$$\xi = \frac{\int_{\theta_c}^{0} (1 + \cos^2(\theta))(\sin\theta)d\theta}{\frac{4}{3}}. \tag{3.15}$$

To obtain the out-coupling efficiency, first the critical angle was determined and then the intensity integrated over the corresponding area.

Since the emission from a PLED structure is not at one certain frequency, the wavelength dependent out-coupling efficiency is necessary for further calculations. The critical angle θ_c is wavelength dependent and has to be calculated for each energy separately. With this data, Eq.3.13 yields values for ξ at every wavelength. The final relation between internal and external quantum efficiency was obtained by integrating $\xi(\lambda)$ over the whole emission spectrum $T(\lambda)$:

$$\xi = \frac{\int_0^\infty \xi(\lambda)T(\lambda)d\lambda}{\int_0^\infty T(\lambda)d\lambda}. \tag{3.16}$$

To determine more accurate IQE values for polymer light emitting devices from measured EQE data compared to the commonly used method with Eq.3.12, this last strategy was applied considering the structure for the polymer layer obtained in this work.

Chapter 4

Chain Conformation in Thin Films of MEH-PPV

poly(2−methoxy, 5−(2'−ethyl−hexyloxy)−p−phenylenevinylene) (MEH-PPV) is the archetypal luminescent polymer film used in optical devices such as polymer light emitting diodes (PLEDs) and microcavity polymer lasers [2, 3]. Typically, thin films of about 100 to 150 nm in thickness are produced by rapid spin casting. For these applications it is important to know the optical properties of the thin films, especially refractive index $n(E)$, dielectric constant $\varepsilon(E)$ and any anisotropy in these parameters. This is crucial when waveguiding is exploited, such as in the case of laser structures, where it is essential to know any preferential orientation of the transition dipole moments. Indications of a degree of anisotropic chain conformation in thin and ultra-thin polymer films were obtained in recent experiments [24, 25, 26, 27, 28]. As the conjugated polymer chains are 'π-stiff' a preferred chain orientation in the surface plane should be not too surprising. For the rigid rod conjugated polymer polypyridine (PPY) it has been shown that a high degree of anisotropy is present in spun cast films [29] and that there is even evidence

for radial order within the ordered layers of polymer chains [30]. However, it is difficult to observe the order found using normal or near normal incidence transmission or reflection measurements. In order to model both, optical constants and optical birefringence, a more complex technique such as variable angle spectroscopic ellipsometry (VASE) as developed by Woollam [31] is required.

Thus, in the first part of this work the possibilities to determine the optical and, from that, structural properties of conjugated polymers by spectroscopic ellipsometry are investigated. This novel technique was applied to thin films of MEH-PPV on silicon wafers besides polarized intensity transmission measurements of MEH-PPV on quartz discs. The film thickness, obtained in the analysis process, varied between 30 and 130 nm but was usually equal for the set of measurements used simultaneously in the regression analysis. These values are in good agreement to the data from thickness profiler measurement of these samples.

Polarized intensity transmission spectra are found to be independent of the polarizer azimuth and any in-plane anisotropy is therefore neglected. Furthermore, measurements of the transition of s to p polarized light and vise versa resulted in very low values for this and thus validated the non-existing in-plane anisotropy. A uniaxial model with the optical axis parallel to the surface normal is used in the analysis process. This model distinguishes only between light propagating parallel to the surface normal and all directions perpendicular to it.

4.1   Optical Constants

In Fig.4.1 are shown the ordinary and extraordinary refraction indices as derived from a point-by-point fit. The extinction coefficients for the ordinary and extraordinary direction are plotted in Fig.4.2. From these extinction coefficients, the absorption coefficient $\alpha = 4\pi k/\lambda$ for k_o can be calculated and is depicted in Fig.4.3 along with the absorption spectrum of a thin MEH-PPV film measured in transmission by assuming $A = 1 - T$ with T for the transmission and A the absorption. The real and imaginary part of the complex dielectric function is shown in Fig.4.4.

In the transparent region (1.24 - 2.10 eV) values of 1.70 to 2.03 for the ordinary refractive index and of 1.50 to 1.55 for the extraordinary one are observed. In the region of non-normal dispersion (2.3 - 2.9 eV) the index of refraction drops down from 2.31 to 1.23 (ordinary) and from 1.59 to 1.48 (extraordinary) respectively. The $\pi - \pi^*$ absorption derived from the ordinary extinction coefficient has an onset at about 2.1 eV and a maximum at 2.5 eV. This peak can also be found for the extraordinary extinction coefficient but with a seven fold reduction in peak intensity.

The uncertainties for this data were calculated from the 90% confidence limit obtained in the analysis process. The errors in the optical parameters for each energy were determined. For the ordinary index of refraction a relative error of less than 1% and for the ordinary extinction coefficient less than 3% was calculated. Larger uncertainties of up to 10% were found for k_o at higher energies close to 5 eV. Utilizable data for the extraordinary optical functions can only be obtained with light polarized parallel to the plane of incidence and at large angles. Since these requirements are only given for a small part of the measured data, the uncertainties for k_e and n_e are higher then for the ordinary functions. The relative errors are up to 2% for n_e and due to the

smaller absolute values up to 35% for k_e. The data for energies greater than about 4.5 eV also slightly depends on the fitting method.
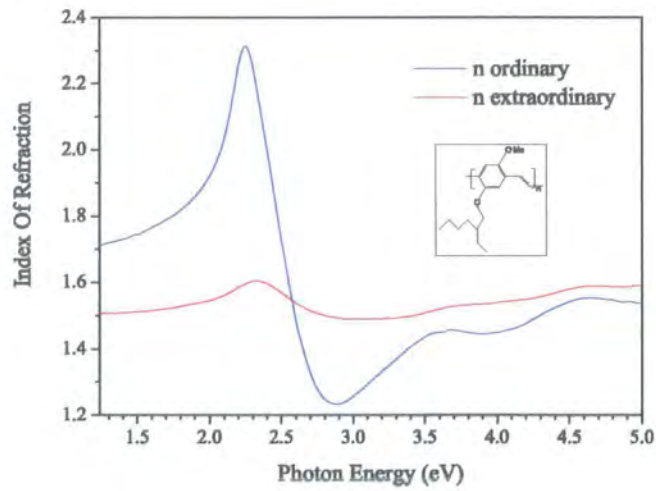
Fig. 4.1: Anisotropic refraction indices of MEH-PPV parallel and perpendicular to the surface normal. Insert: chemical structure of MEH-PPV
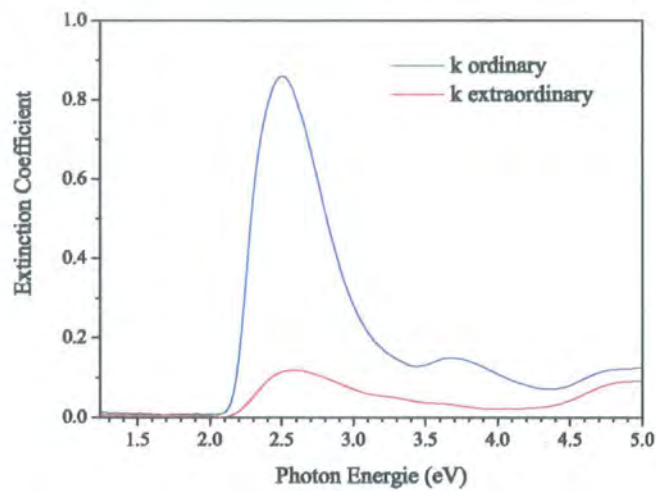
Fig. 4.2: Anisotropic extinction coefficients of MEH-PPV parallel and perpendicular to the surface normal.
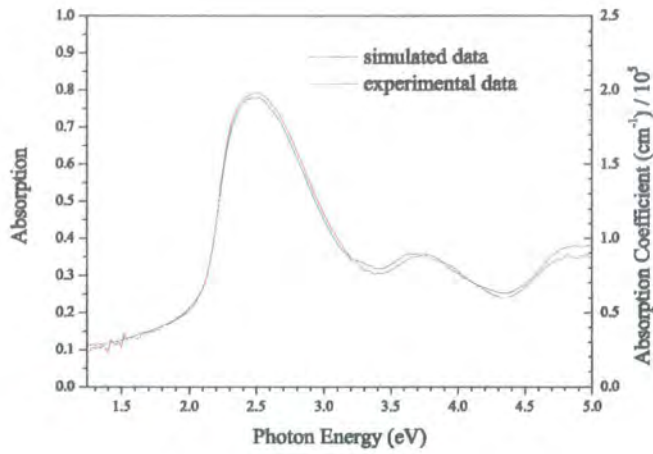
Fig. 4.3: Comparison between simulated absorption data calculated from the ordinary extinction coefficient and the experimental absorption data of MEH-PPV. The simulated data is also shown in units of the absorption coefficient $\alpha = 4\pi k/\lambda$.
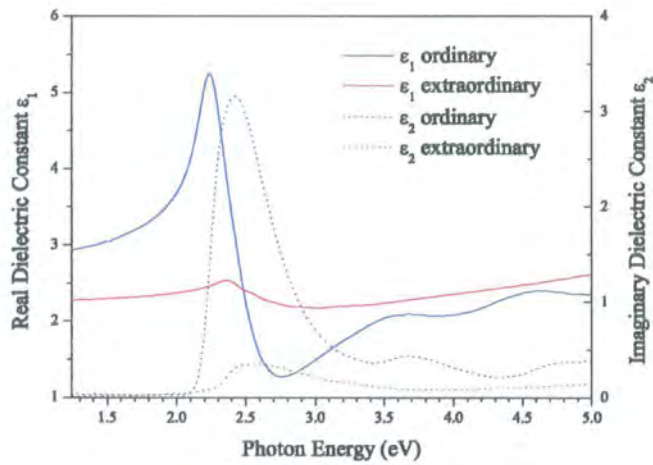
Fig. 4.4: Real (solid line) and imaginary part (dotted line) of the anisotropic dielectric function of MEH-PPV parallel and perpendicular to the surface normal.

4.2   Degree of Anisotropy

For this kind of uniaxial material an angular distribution function as the ratio between the $\pi - \pi^*$ absorption parallel to the surface plane and the total $\pi - \pi^*$ absorption can be defined [24]:

$$d_{\pi\parallel} = \frac{1}{1 + k_e/2k_o}.$$ (4.1)

Compared to an isotropic layer ($k_e = k_o$) which yields a value of $d_{\pi\parallel} = 2/3$ and a perfect uniaxial system with no extraordinary absorption $d_{\pi\parallel} = 1$, the calculated average value for MEH-PPV in the spectral range of the $\pi - \pi^*$ absorption (2.2 eV to 3.3 eV) is 0.91.

Similar measurements were also performed on samples annealed at $80°C$ for 12 h in a vacuum oven i.e. above the glass-transition temperature of $65°C$ [32] to check for modification in the chain alignment after such a treatment. No relevant change in the spectra of the annealed samples and the degree of anisotropy was observed.

4.3   Implication on Chain Conformation

The extracted indices of refraction as a macroscopic optical response correspond to the macroscopic average orientation of the polymer chains in the film. The observation of such high anisotropy, with a ratio between the absorbance at the $\pi - \pi^*$ transmission energy in the ordinary and extraordinary direction of seven, is therefore explained by a preferred parallel orientation of the polymer chain backbones to the surface plane. Because of the absence of in-plane anisotropy in the experiments carried out, a random orientation of the chains in the plane of surface is expected. It should be noticed that the light beam diameter, of about 3 mm, used in the polarized transmission

measurements, causes a certain degree of averaging and it is not possible to completely rule out any in-plane anisotropy, as observed in PPy [30].

The ability of MEH-PPV to form such highly ordered structures is ascribed to the polymer being rather π stiff, so having rigid rod character. The long, rather stiff chains are forced to take a formation parallel to the surface plane by rapid spin casting and this yields a uniaxial optical responde.

Chapter 5

Optical Anisotropy in Thin Films of Polyfluorene and its Effect on the Out-coupling of Light in Typical PLED Structures

5.1 Optical Properties of PF2/6am5

One of the most commonly used conjugated polymer is the blue emitting $poly(9, 9 - dioctylfluorene)$ (PFO). This polymer and other poly(fluorene)s are promising for light-emitting diode applications due to their increased oxygen stability and their high charge carrier (holes, in the case of PFO) mobility of around 4×10^{-4} cm^{2}V^{-1}s^{-1} [33]. The amine endcapped PFO derivative $\alpha, \omega - Bis[N, N - di(5 - methylphenyl)aminophenyl] - poly(9, 9 - bis(2 - ethylhexyl)fluoren - 2, 7 - diyl)$ (PF2/6am5) was introduced to minimize

excimer formation in spin cast films [34, 35] and was found to be highly ef-
ficient as an active layer in PLEDs [36]. Thus, the optical properties of thin
films of this material were determined to be able to discus the light prop-
agation and out-coupling in such devices. Spectroscopic ellipsometry and
polarized intensity transmission data was acquired for PF2/6am5 films on
silicon wafers and quartz discs. The film thickness, obtained in the analy-
sis process, varied between 70 and 80 nm. Thickness profiler measurement
validated these values.

5.1.1   Optical Constants

The index of refraction of 70 nm thick PF2/6am5 films in the spectral range
of 1.24 eV and 5 eV is presented in Fig.5.1 and the anisotropic extinction
coefficient in Fig.5.2. From this data, the absorption coefficient $\alpha = 4\pi k/\lambda$
for k_o is calculated and depicted in Fig.5.3 along with the absorption spec-
trum of a thin PF2/6am5 film measured in transmission ($A = 1 - T$). The
real and imaginary part of the complex dielectric function in ordinary and
extraordinary direction is shown in Fig.5.4.

At the absorption band of PF2/6am5 between ca. 410 nm (3.0 eV) and
330 nm (3.8 eV) the ordinary index of refraction drops from 2.1 down to 1.3
while in the transparent region the value converges to ca. 1.6. This non-
normal dispersion is less strong for the extraordinary index of refraction,
which is probed by light perpendicular to the surface normal. The maxi-
mum and minimum values are ca. 1.65 and 1.55 respectively. This high
anisotropic optical response is also seen in the relation between ordinary and
extraordinary absorption. Light at a wavelength of 380 nm is adsorbed six
times stronger if it is propagating parallel to the surface normal compared
to perpendicular to it.

The 90% confidence, limit obtained in the analysis, provides the error of each fitting parameter and, by applying a point by point fit, the error of the optical functions at every wavelength. For the ordinary index of refraction a relative error of less than 0.5% and for the ordinary extinction coefficient less than 2% was calculated. Larger uncertainties of up to 10% were found for k_o at higher energies close to 5 eV. Utilizable data for the extraordinary optical functions can only be obtained with light polarized parallel to the plane of incidence and at large angles. Since these requirements are only given for a small part of the measured data, the uncertainties for k_e and n_e are higher then for the ordinary functions. The relative errors are up to 2% for n_e and due to the smaller absolute values up to 35% for k_e. The data for energies higher than about 4.5 eV also slightly depends on the fitting method.
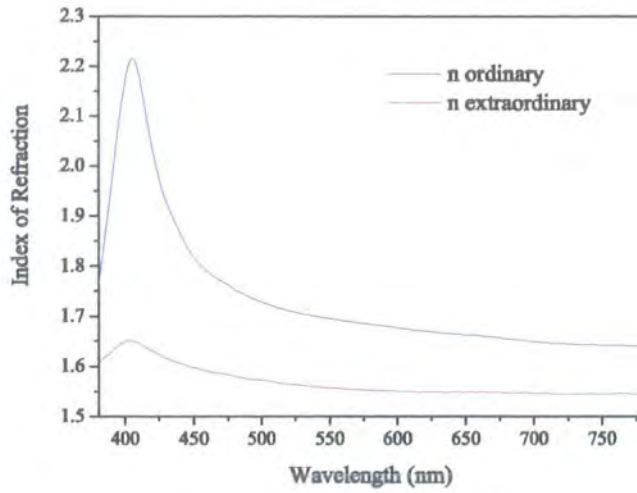
Fig. 5.1: Anisotropic refraction indices of PF2/6am5 parallel and perpendicular to the
surface normal.
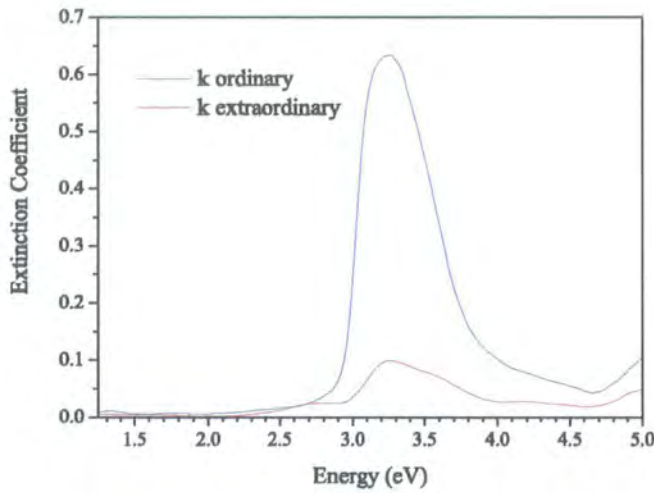
Fig. 5.2: Anisotropic extinction coefficients of PF2/6am5 parallel and perpendicular to
the surface normal.

Fig. 5.3: Comparison between simulated absorption data calculated from the ordinary
extinction coefficient and the experimental absorption data of PF2/6am5. The simulated
data is also shown in units of the absorption coefficient $\alpha = 4\pi k/\lambda$.
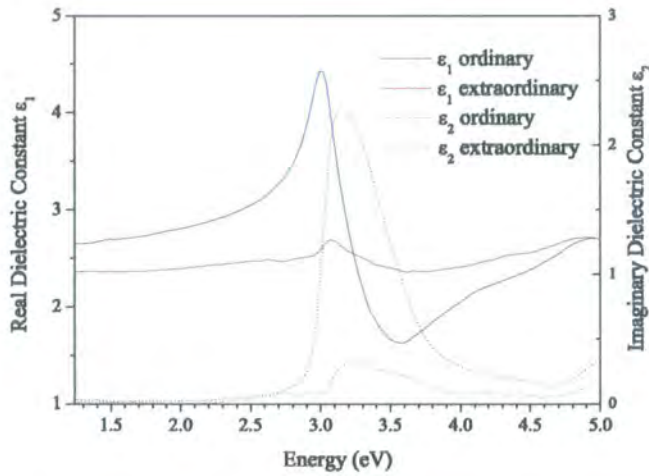
Fig. 5.4: Real (solid line) and imaginary part (dotted line) of the anisotropic dielectric
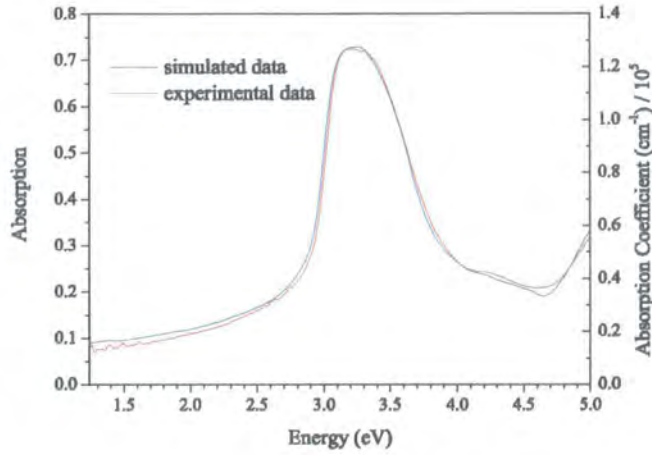function of PF2/6am5 parallel and perpendicular to the surface normal.

5.1.2 Anisotropy in PF2/6am5 Films

The angular distribution function as the ratio between the $\pi - \pi^*$ absorption parallel to the surface plane and the total $\pi - \pi^*$ absorption (Eq.4.1) is calculated in the spectral range of this absorption between 2.8 and 4.0 eV. The resulting average value of $d_{\pi\|} = 0.88$ is fairly close to the value for maximal anisotropy of 1 and significantly higher than 2/3, which is the value for perfect isotope materials. At the wavelength of maximum absorption the extinction coefficient for light propagating parallel to the surface normal is almost seven times higher than for perpendicular directions. A highly ordered system with chain alignment in the plane of surface is therefore admissible for the modelling of processes in devices.

5.2 Influence of Anisotropic Optical Properties to Light Out-Coupling in PLEDs

In the previous section it is shown that even semi rigid-rod conjugated polymers can form highly anisotropic thin films when spun cast (with rapid solvent evaporation). This property of thin spun cast films will have important ramifications on the performance of polymer light emitting devices where waveguiding of light within the device structure strongly determines the amount of light which escapes the device in the forward direction, i.e. that which is useful in the application. Greenham *et al* made the first estimates for light out-coupling in devices and deduced a relationship between internal (IQE) and external (EQE) electroluminescence quantum efficiency, e.g. IQE $\approx 0.5n^{-2}$ EQE [21]. More recently this group has revisited this problem and published an article discussing out-coupling in more detail [20]. In this

section, the new model is used as a starting point to observe what effects thin film anisotropy have on the amount of light coupled out of the device, and it is determined how a strongly varying refractive index over the emission wavelengths affects this. Further it is shown, what effect shifting emission well away from the region of non-normal dispersion has on out-coupling, such as occurs in devices doped with a dye sensitizer [36, 37, 38, 39].

All external quantum efficiency and electro luminescence measurements, used in this work, were carried out by R.W.T. Higgins who also fabricated the polymer light emitting diodes for this experiment.

PLEDs where produced from the conjugated polymer $\alpha, \omega - Bis[N, N - di(4-methylphenyl)aminophenyl] - poly(9, 9 - bis(2 - ethylhexyl)fluoren - 2, 7 - diyl)$ (PF2/6am4) or $2, 3, 7, 8, 12, 13, 17, 18 - octaethyl - 21H, 23H - porphyrin\ platinum(II)$ (PtOEP) doped PF2/6am4. The doping level was 0.5, 2 and 4% of PtOEP in PF2/6am4. These polymers were spin coated as a 100 nm thick active layer for the device. A more detailed description of the PLED preparation process can be found in [37].

The PFO type PF2/6am5, which optical functions are presented in section 5.1, should have highly comparable optical properties to PF2/6am4 due to only slightly changes in the concentration of amine end-groups between these two polymers. The application of the optical functions of PF2/6am5 for calculations with layers of PF2/6am4, carried out in this section, is therefore justifiable.

5.2.1 EQE in PtOEP doped PF2/6am4 PLEDs

The external quantum efficiency data, refereed in this work, was obtained by measuring the total photon energy emitted in an certain angular range from the device. By assuming an Lambertian emission from the surface of the

PtOEP (%)		0	0.5	2	4
Current Density (mA/cm^2)		70.7	15.6	1.9	7.8
Peak EQE (%)		1.2	2.4	2.0	1.3

Table 5.1: EQE for undoped and PtOEP doped PF2/6am4 PLEDs and the current density during the measurement (data from [37])

PLED, the total photon energy, escaping through the surface, was calculated. By adjusting the bias on the PLED, the best EQE value was determined. The highest values for each doping level are listed in Tab.5.1 together with the current density at which the efficiency was obtained.

5.2.2   IQE in PtOEP doped PF2/6am4 PLEDs

Like seen in the graph for the isotropic extinction coefficient (Fig.5.2), thin films of PF2/6am5 exhibit fairly high in-plane alignment of its molecule chains. By assuming an even perfect in-plane alignment of all dipoles, the wavelength dependent out-coupling efficiency $\xi(\lambda)$ can be determined by Eq.3.7 using the angle dependent intensity distribution for the light emission as in Eq.3.14 and the data for the anisotropic index of refraction of PF2/6am5. The values for the out-coupling are depicted in Fig.5.5. The differences in ξ for different wavelength are remarkable, i.e. the out-coupling efficiency is highly dependent of the emission wavelength. At 400 nm, only 19% of the generated light can leave the device (regarding to this simple model) but up to 30% of the infrared light at wavelengths higher than ca. 700 nm. In Fig.5.6 the emission spectrum for PF2/6am4 with broad emission lines between 400 nm and around 550 nm is shown. The integration of $\xi(\lambda)$ over this emission spectrum yields a out-coupling constant of $\xi = 0.257$.

Since devices made from PtOEP doped PF2/6am4 show an increase of their
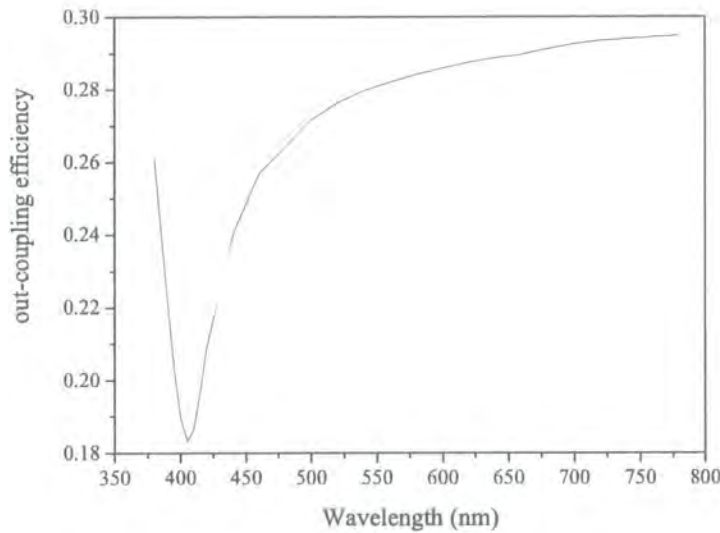
Fig. 5.5: Wavelength dependent out-coupling constant ξ for PF2/6am5

EQE values, the influence of changed optical and optoelectronical proper-
ties on this effect has to be observed. Analogously to the doped PF2/6am4
samples, the optical functions of PtOEP doped PF2/6am5 are determined
for doping levels of 0.5, 2 and 4%. The index of refraction, extinction co-
efficient and anisotropy is not affected by doping and the dispersion data
shown in section 5.1 is valid for all devices. Therefore, the shifted electro
luminescence emission spectrum through doping, depicted in Fig.5.6, is the
remaining factor which has to be considered in the calculation of the internal
quantum efficiency for all devices. The EL spectrum of 0.5% PtOEP doped
PF2/6am4 is almost completely shifted to the sharp dopant EL emission
band around 645 nm and only a small amount of emission is visible at the
position of the undoped polymer. The spectra for other doping levels is not
shown in Fig.5.6 because of a highly comparable shape to the doped sample
depicted.

The calculation of the out-coupling efficiency for the different doped devices,
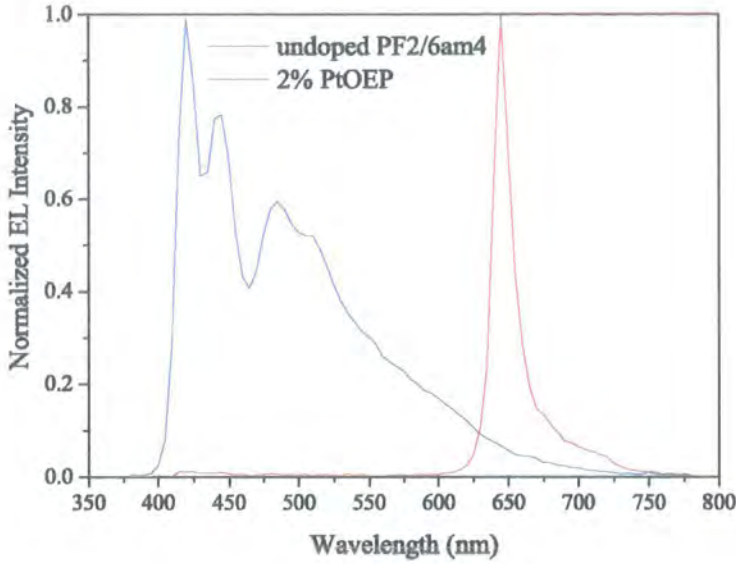
Fig. 5.6: Electro luminescence emission spectrum of undoped PF2/6am4 and PF2/6am4
doped with 2% PtOEP.

PtOEP (%)	0	0.5	2	4
ξ	0.257	0.283	0.288	0.288
Peak EQE (%)	1.2	2.4	2.0	1.3
Peak IQE (%)	4.6	8.3	6.9	4.5

Table 5.2: IQE for undoped and PtOEP doped PF2/6am4 PLEDs

according to Eq.3.16 in section 3.4.3, yields the values shown in Tab.5.2. An
increase of the out-coupling efficiency of up to 12% by doping is noticed only
because of the changed emission frequency. For higher doping levels, the
effect of an increasing out-coupling is not present due to identical emission
spectra. From the values of the external quantum efficiency, the IQE values
in the doped devices are determined and also presented in Tab.5.2. These cal-
culations, taking account of refractive index dispersion and anisotropy, yield
reduced values of IQE, compared to the simple $0.5n^{-2}$ relationship mentioned

in section 3.4.2, e.g. for the pure PF2/6am5 case taking $n = 1.6$ the simple model gives $\xi = 0.195$ (IQE, 6.14%) or taking $n = 2$ gives $\xi = 0.125$ (IQE, 9.6%) whereas this model yields a more realistic value of $\xi = 0.257$ (IQE, 4.6%).

The IQE of the most efficient PtOEP doped sample is only 80% higher than of the pure PF2/6am5. The photo luminescence quantum yield (PLQY) of the used PF2/6am5 is 0.24 [40] whereas that of PtOEP is around 0.5 [41], thus the PLQY of the dye is twice that of the host polymer and so accounts for all the increase in the internal efficiency of the doped device. This finding agrees well with recent results which show that all emission in PtOEP doped devices arises from charge recombination at the dye as the dye is a very efficient charge trapping site [38] and the fact that the polymer triplet lifetime at room temperature is very short [40]. Thus, for polymers it seems that such heavy atom sensitizers simple act as efficient charge recombination sites only.

Chapter 6

Effect of Chain Rigidity on Photophysical Properties of Pyridine-based Luminescent Polymers

Conjugated polymers exhibit a variety of advantages for the application in light emitting diodes. However, there is still concern over the oxidative and photo-stability of the active polymers in such devices. The minimum lifetime requirement, demanded by industry, of 10,000 hours is very difficult to attain in luminescent polymers. The reason for the oxidative instability of conjugated polymers arises from the electron rich π orbitals which are relatively easy to remove by oxidizing agents. Thus, there is a need for more stable luminescent polymers which are still highly efficient and can be processed in the same simple fashion as the current materials. The requirement of making the oxidation more difficult is in contrast to still retain sufficient π electron density to impart the desired physics e.g. high charge carrier mobil-

ity, high emission efficiency and work function compatibility with common electrode materials. One way to achieve such properties is to remove electron density from the (phenyl) repeat units along the polymer backbone whilst retain π conjugation by the introduction of nitrogen heteroatoms into the π system of the repeat unit i.e. into a phenyl ring as in the case of poly(2,5-pyridinediyl) (PPy) which is investigated in this chapter. These properties were first elucidated by Yamamoto et al [42], not only did he show that PPy (and substituted variants of the polymer) is luminescent, but also that it is very stable with respect to oxidation even under severe conditions. PPy is a simple rigid rod conjugated polymer, soluble in formic acid, which allows the use of many spectroscopic techniques to study it.

Solid PPy emits in the green part of the spectrum. By introducing meta linkages into the chain (see Fig.2), the emission is shifted to blue. These linkages add non-conjugation nodes and therefore can break conjugation. These breaks are expected to raise the $\pi - \pi^*$ transition energy and a blue shift in emission should be noticeable. For this purpose, a fully meta poly(2,6-pyridinediyl) (PmPy) was synthesized by Dr. Lockhart Horsburgh next to different copolymers with a variable number of random meta linkages. Ellipsometry measurements were made on thin films of $para$ PPy, $meta$ PmPy and different copolymers of these materials and compared with light scattering data provided by Prof. Hugh D. Burrows.

Optical measurements were made on thin films spun on fused silica substrates for transmission measurements and onto Si substrates with oxide layers of 2 to 120 nm for ellipsometry studies. A film thickness of 30 to 45 nm was obtained in the analysis process and checked by thickness profiler measurements.

6.1 Optical Properties of PPy and PmPy

The refractive indices of PPy with different *meta* PmPy (0%, 18% and 100%) ratios in the ordinary and extraordinary direction as derived from a point-by-point fit of the ellipsometry data are shown in Fig.6.2 after diagrams of the chemical structure of PPy, PmPy/PPy copolymers and PmPy (Fig.6.1). The extinction coefficient of the same polymers for light polarized parallel and perpendicular to the plane of incidence are plotted in Fig.6.3. For the pure PPy, the complex dielectric function is depicted in Fig.6.4. Absorption data for some copolymers measured in transmission ($A = 1 - T$) is presented in Fig.6.6. In the transparent region of pure PPy (1.24 - 2.70 eV) values of 1.9 to 2.5 for the ordinary refractive index and of 1.8 to 2.1 for the extraordinary one are observed. In the region of non-normal dispersion (2.9 - 3.8 eV) the index of refraction drops down from 3.1 to 1.7 (ordinary) and from 2.5 to 1.4 (extraordinary) respectively in this material. The $\pi - \pi^*$ absorption derived from the ordinary extinction coefficient has an onset at about 2.7 eV and a maximum at 3.2 eV (387 nm) in the pure PPy as expected from past publications [43]. This peak is also visible in the extraordinary direction but is very weak with a low maximum value of the extinction coefficient of 0.05. All samples with fractions of meta linkages exhibit a blue shift of the maximum absorbtion wavelength dependent of the ratio of the mPy monomer unit and a weaker difference in the extinction coefficients for the ordinary and extraordinary direction, k_o and k_e. The maximum values for k_o are 1.0 for 18% *meta* and 0.4 for pure PmPy. This decrease of ordinary absorption is connected to an increase in the extraordinary direction. The values for these extinction coefficients going up to 0.2 for 18% and 0.3 for 100% PmPy.

The 90% confidence limit for each fitting parameter and by processing a point-by-point fit for every wavelength is calculated by the analysis software.

For the refractive index of PPy, this error is less than 1% and for the ordinary part of the extinction coefficient less than 2%. Only in the transparent region are the relative uncertainties higher due to small absolute values. For the same reason the relative error for the extraordinary part of the extinction coefficient is about 50% and higher.
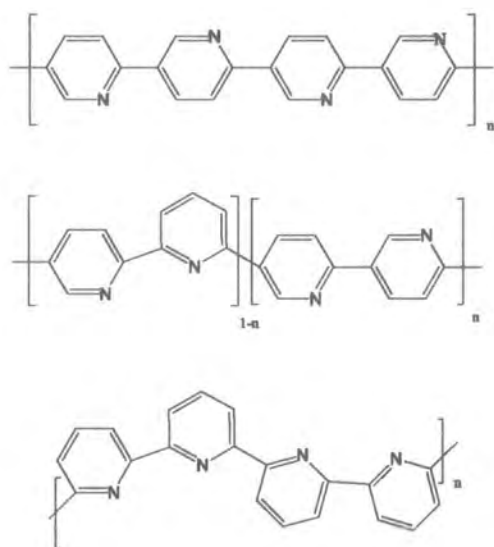
Fig. 6.1: Schematic diagrams of the pyridine polymer structures; top, PPy, middle, *meta-para* co-polymer, bottom, PmPy
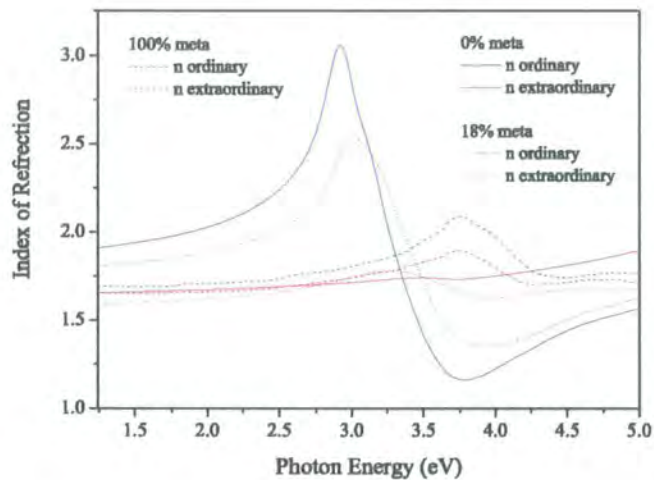
Fig. 6.2: Anisotropic refraction indices of thin films from pure PPy, PPy with 18% PmPy and pure PmPy parallel and perpendicular to the surface normal. Insert: chemical structure of PPy

Fig. 6.3: Extinction coefficients of thin films from pure PPy, PPy with 18% PmPy and pure PmPy parallel and perpendicular to the surface normal.
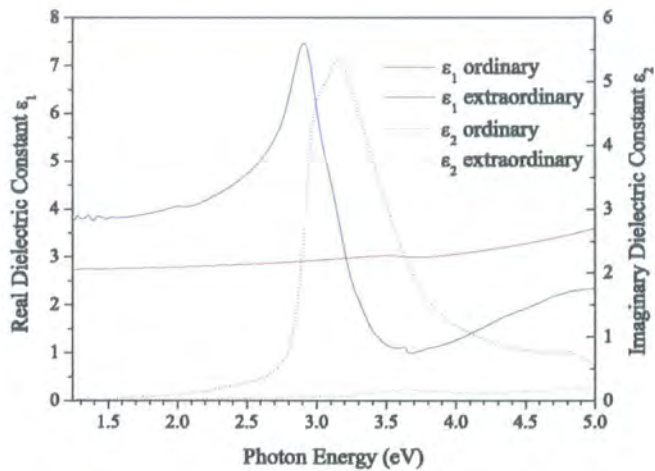
Fig. 6.4: Real (solid line) and imaginary part (dotted line) of the anisotropic dielectric function of PPy parallel and perpendicular to the surface normal.

% of PmPy	0	18	25	35	42	100
$d_{\pi\parallel}$	0.966	0.880	0.873	0.835	0.792	0.664

Table 6.1: Angular distribution function (Eq.4.1) in the spaectral range of the $\pi - \pi^*$ absorption for PPy with different ratios of PmPy

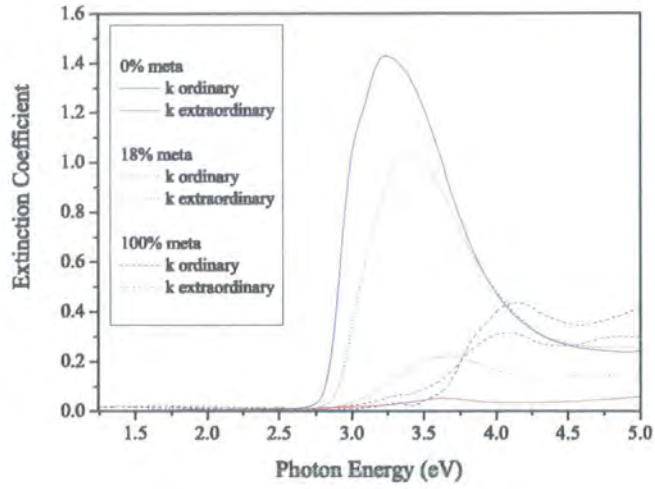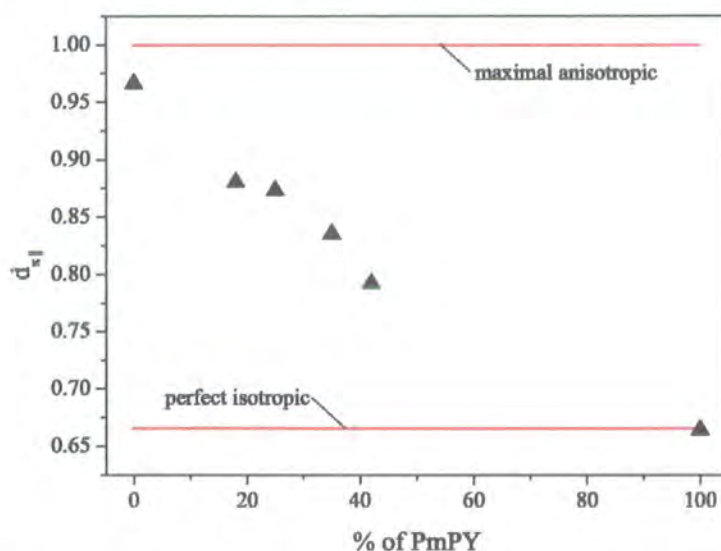**Fig. 6.5:** Angular distribution function in the spaectral range of the $\pi - \pi^*$ absorption for PPy with different ratios of PmPy

6.2 Anisotropy in PPy and PmPy Films

An angular distribution function for a uniaxial material as the ratio between the $\pi - \pi^*$ absorption parallel to the surface plane and the total $\pi - \pi^*$ absorption is defined in Eq.4.1. For six different copolymers of PPy with PmPy, this distribution is calculated by using an average extinction coefficient in the spectral range of the $\pi - \pi^*$ absorption (2.75 eV to 4.5 eV for PPy or 3.4 eV to 4.6 eV for PmPy) obtained in the fitting process and is listed in Tab.6.1 and depicted in Fig.6.5. For the pure PmPy an almost perfect isotropic optical response with a distribution value very close to the ideal value of 2/3

is obtained. This is an enormous difference to PPy with its strong isotropic distribution almost reaching the theoretical value of 1.

As already discussed in section 4.2, the degree of anisotropy in thin films of conjugated polymers can be linked to the amount of order in the film. Thus, the highly rigid rod polymer PPy with a strong uniaxial anisotropic behavior is almost perfectly oriented parallel to the substrate but with no order within the layer. The reduction of anisotropy in copolymers with a higher mPy monomer ratio gives an indication for a change in stiffness of the polymer backbone. The isotropic optical response of pure PmPy suggests a coiled conformation of the polymer chains even when spun cast onto the substrate. These findings show very dramatically how the meta linkages change the stiffness of the molecule chain and give it a higher flexibility.

6.3 Absorbance Data

Further validation of a broken conjugation length in PmPy and the possibility to tailor this property with a variable ratio of the monomer unit of mPy in the pyridine copolymer is given by separate transmission measurements and the absorption spectra ($A = 1 - T$) are depicted in Fig.6.6. The wavelengths of maximal absorption for the created copolymers are listed in Tab.6.2. For only low concentrations of the mPy monomer in the copolymer, the absorbtion spectrum does not change remarkable, but starting at ca. 35% of mPy a continuous shift to blue wavelengths is visible for a increasing mPy ratio. Starting with 387 nm for pure PPy, the absorption maximum for PmPy is at 303 nm. This $\pi - \pi^*$ transmission energy increase, visualized in the blue shifted absorption, implicates a structure change from rigid rod like behavior to coiled chains since a coiled conformation results from less π-stiffness due

% of PmPy	0	18	25	35	42	50	100
$\lambda_{max}(nm)$	387	365	367	367	330	323	303

Table 6.2: Absorption maximum wavelengths of pyridine copolymer films.
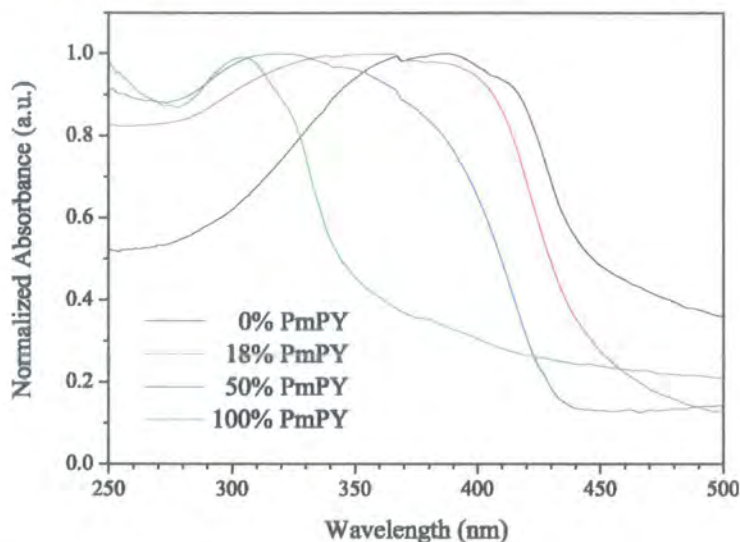
Fig. 6.6: Absorption data for pyridine copolymer films with a different ratio of PmPy.

to a distortion in the conjugation. The shorter the conjugation of the orbitals
along the chain is, the higher is the 'band gap' for a $\pi - \pi^*$ transition and
only a perfect conjugation of all π orbitals of the chain results in the lowest
possible energy gap.

6.4   Light Scattering Data

Dynamic light scattering (DLS) measurements were made on solutions (0.04
- 0.2 wt%) of the polymers in formic acid by Prof. Hugh D. Burrows. Large
depolarization was observed in DLS experiments on solutions of the pure
para PPy. Although it was not possible to measure the degree of depolar-
ization with the system used, the results strongly suggest that the polymer

exists as a large, very rigid rod. Bimodal relaxation time distributions for the scattered light were observed for all cases which are likely to be due to translational (slow mode) and predominantly rotational (fast mode) diffusion of rigid rod molecules in the solution.

From the decay of the slow component, a translational diffusion coefficient D was calculated for each system. For the *para* PPy samples, the measured translation diffusion coefficients were essentially independent of polymer concentration and sample. A value $D = 3.45 \pm 0.39 \times 10^{-12}$ m^{2}s^{-1} was obtained for the translational diffusion. From the modified Stokes-Einstein relationship, $R_H = k_T/6\pi\eta_0 D$ (where η_0 is the solvent viscosity, 1.607 mPa s), a hydrodynamic radius of $R_H = 40 \pm 4$ nm was obtained for *para* PPy.

The fast mode is dominated by rotation of the rigid rod polymers, and the rotational diffusion coefficient Θ. The values determined for the rotational diffusion did not depend significantly on either concentration or polymer, and a value of $\Theta = 4.39 \times 10^5$ s^{-1} was determined for rotational diffusion of *para* PPy in formic acid. This can be related to the length L and diameter d of a rigid rod by Broersma's relationship [44]. The measured rotational diffusion coefficient gives a value of L in the range 34.5 - 38.5 nm, in good agreement with the translational diffusion data, confirming the almost rigid rod nature of PPy.

These DLS studies were also made on solutions in formic acid of *poly(2, 6 − pyridinediyl)* for comparison. The PmPy also showed fast and slow relaxation times, from which rotational and translational diffusion coefficients of $\Theta = 7.97 \pm 0.39 \times 10^5$ s^{-1} and $D = 6.89 \pm 0.73 \times 10^{12}$ m^{2}s^{-1} were calculated. These are rather higher than the values for PPy but for a comparable molecular weight, and may suggest shorter rod lengths. From the above data, a hydrodynamic radius of $R_H = 20 \pm 2$ nm could be estimated. Thus, the

DLS measurements shall be deemed to be an additional indicator for the coil nature of PmPy.

For solutions made from copolymers containing 18% and 35% of the $2, 6 - pyridinediyl$ monomer, the DLS measurements show a more complicated relaxation distribution which results from the different chain segments and their difficult to analyze kinetic behavior. Results obtained by applying the same analysis procedure used in the pure PPy and PmPy case are therefore not suited for a direct comparison.

To sum up, PPy is a highly rigid rod conjugated polymer as validated by DSL studies and forms almost perfectly layered films with chain alignment parallel to the plane of surface when spun cast with rapid solvent evaporation as seen in the anisotropic optical response. For PmPy, the DSL data indicates a more coil like conformation and spin casting results in isotropic films. Therefore, the chain orientation in thin films is clearly dominated by the chain rigidity.

Chapter 7

Conclusion

In this work, the results of variable angle spectroscopic ellipsometry measurements of thin films of conjugated polymers are presented. A non-linear regression analysis of the data obtained allows for the first time a determination of the anisotropic optical functions of the polymer layers in a broad spectral range with high accuracy. The optical response of the polymer films, made from solutions spun cast onto plain substrates, was found to be uniaxial with the optical axis parallel to the surface normal. Two complex indices of refraction are therefore necessary to discuss light propagation in the layer parallel to the plane of surface as well as perpendicular to it. For the conjugated polymer MEH-PPV, the anisotropy in these indices was found to be surprisingly high, i.e. the direction of propagation has a remarkable influence on refraction and absorption of light in thin films of this material. Light at a wavelength of the peak of the $\pi - \pi^*$ transition is absorbed about seven times more strongly if it is propagating parallel to the surface normal compared to perpendicular to it. Since the direction of the dipole moment for this transition in conjugated polymers is assumed to be along the molecule chain, this finding implicates a preferred chain alignment in the plane of surface. The

molecule chain of MEH-PPV is usually considered to be less rigid rod like but the ellipsometry studies show, that even semi rigid rod molecules form highly ordered films when spun cast with rapid solvent evaporation. This fact is very important for the design of PLEDs or Laser structures where out-coupling and waveguiding are the vital processes and only proper knowledge of the optical functions allows to model these effects and to optimize the device.

For light emitting diodes made from PF2/6am4, a derivative of the commonly used PFO, the influence of the anisotropic and highly dispersive index of refraction on the amount of light capable to couple out of the device was investigated to point out the importance of the data obtainable by ellipsometry. It could be shown, that the out-coupling efficiency is highly dependent on the emission wavelength especially if the emission is shifted away from the region of high dispersion. Differences of more than 50% in the out-coupling efficiency were calculated for different wavelengths. For PtOEP doped PF2/6am5 samples, which exhibit a red shifted emmision compared to the undoped devices, the internal quantum efficiency was calculated by using the results for the out-coupling efficiency. These results from accurate optical data were compared to results obtained by applying the commonly used approximation which assumes e.g. $n = $ const. $= 2$. The IQE values were found to be up to 100% higher if the simple constant index of refraction is applied. This can lead to misunderstanding of internal processes if very high internal efficiency is estimated which does not exist and ellipsometry data is helpful to avoid such problems. However, The increased external efficiency of the PF2/6am5 devices by doping with PtOEP was fully accounted by the increased out-coupling efficiency and a higher photoluminescence quantum yield of the dye.

Furthermore, the ability of ellipsometry to monitor structural changes in conjugated polymers by using the influence of these changes to the photophysical properties was demonstrated. The perfect rigid rod conjugated polymer PPy, as validated by dynamic light scattering data, forms highly anisotropic films with almost no absorbance in the directions along the plane of surface. Thus, the π-stiffness of the chains results in a perfectly aligned conformation when spun cast. For the polymer PmPy, which has meta linkages (compared to PPy), DSL studies suggest a coiled conformation of the chain because of a dramatically increased chain flexibility by the meta links. The analysis of ellipsometry data from thin films of PmPy yields an almost isotropic optical behavior and no preferred chain orientation in the layer was therefore assumed. For copolymers created from the monomer units mPy and Py, the amount of anisotropy in thin films is directly connected to the ratio of the meta content which leads to the conclusion, that the chain orientation is dominated by chain rigidity. The reason for the loss of chain rigidity by introducing *meta* links in the molecule was found in the absorption spectra. The blue shift for higher *meta* content results from a raised $\pi - \pi^*$ transition energy. A broken conjugation of the π orbitals by *meta* links is a likely explanation for this effect and yields a disappearance of π-stiffness.

Thus, ellipsometry is a very powerful and important tool to study conjugated polymers. The results of such measurements are essential for the design of high efficiency optical devices and this method will therefore become a standard procedure for research in this field.

Bibliography

[1] J. H. Burroughes, D. D. C. Bradley, A. R. Brown, R. N. Marks, K. Mackay, R. H. Friend, P. L. Burns, and A. B. Holmes. Light-emitting-diodes based on conjugated polymers. *Nature*, 347(6293):539–541, 1990.

[2] A. J. Heeger. Light emission from semiconducting polymers: Light-emitting diodes, light-emitting electrochemical cells, lasers and white light for the future. *Solid State Communications*, 107(11):673–679, 1998.

[3] N. Tessler, G. J. Denton, and R. H. Friend. Lasing from conjugated-polymer microcavities. *Nature*, 382(6593):695–697, 1996.

[4] K. Schillen, W. Brown, and R. M. Johnsen. Micellar sphere-to-rod transition in an aqueous triblock copolymer system - a dynamic light-scattering study of translational and rotational diffusion. *Macromolecules*, 27(17):4825–4832, 1994.

[5] E. Alami, M. Almgren, W. Brown, and J. Francois. Aggregation of hydrophobically end-capped poly(ethylene oxide) in aqueous solutions. fluorescence and light-scattering studies. *Macromolecules*, 29(6):2229–2243, 1996.

[6] John David Jackson. *Classical electrodynamics*. Wiley, New York ; Chichester [England], 3rd edition, 1999.

[7] Bahaa E. A. Saleh and Malvin Carl Teich. *Fundamentals of photonics.* Wiley series in pure and applied optics. Wiley, New York, 1991.

[8] *Guide to Using WVASE32.* J. A. Woollam Co., Inc.

[9] M. Schubert, B. Rheinlander, J. A. Woollam, B. Johs, and C. M. Herzinger. Extension of rotating-analyzer ellipsometry to generalized ellipsometry: Determination of the dielectric function tensor from uniaxial tio2. *Journal of the Optical Society of America a-Optics Image Science and Vision,* 13(4):875–883, 1996.

[10] L. A. A. Pettersson. *Optical modeling and characterization of layers and multilayer structures.* PhD thesis, Linkpings universitet, 1999.

[11] M. L. Shand, R. R. Chance, M. Lepostollec, and M. Schott. Raman photoselection and conjugation-length dispersion in conjugated polymer-solutions. *Physical Review B,* 25(7):4431–4436, 1982.

[12] N. T. Harrison, G. R. Hayes, R. T. Phillips, and R. H. Friend. Singlet intrachain exciton generation and decay in poly(p- phenylenevinylene). *Physical Review Letters,* 77(9):1881–1884, 1996.

[13] L. J. Rothberg, M. Yan, F. Papadimitrakopoulos, M. E. Galvin, E. W. Kwock, and T. M. Miller. Photophysics of phenylenevinylene polymers. *Synthetic Metals,* 80(1):41–58, 1996.

[14] J. M. G. Cowie. *Polymers: chemistry and physics of modern materials.* Blackie ; Chapman and Hall, Glasgow New York, 2nd edition, 1991.

[15] Rudolf Ernst Peierls. *More surprises in theoretical physics.* Princeton series in physics. Princeton University Press, Princeton, N.J., 1991.

[16] P. W. Atkins. *Molecular quantum mechanics*. Oxford University Press, Oxford [Oxfordshire] ; New York, 2nd edition, 1983.

[17] J. R. Sheats, H. Antoniadis, M. Hueschen, W. Leonard, J. Miller, R. Moon, D. Roitman, and A. Stocking. Organic electroluminescent devices. *Science*, 273(5277):884–888, 1996.

[18] A. C. Arias, M. Granstrom, K. Petritsch, and R. H. Friend. Organic photodiodes using polymeric anodes. *Synthetic Metals*, 102(1-3):953–954, 1999.

[19] C. M. Herzinger, B. Johs, W. A. McGahan, J. A. Woollam, and W. Paulson. Ellipsometric determination of optical constants for silicon and thermally grown silicon dioxide via a multi-sample, multi- wavelength, multi-angle investigation. *Journal of Applied Physics*, 83(6):3323–3336, 1998.

[20] J. S. Kim, P. K. H. Ho, N. C. Greenham, and R. H. Friend. Electro-luminescence emission pattern of organic light-emitting diodes: Implications for device efficiency calculations. *Journal of Applied Physics*, 88(2):1073–1081, 2000.

[21] N. C. Greenham, R. H. Friend, and D. D. C. Bradley. Angular-dependence of the emission from a conjugated polymer light-emitting diode - implications for efficiency calculations. *Advanced Materials*, 6(6):491–494, 1994.

[22] M. H. Lu and J. C. Sturm. External coupling efficiency in planar organic light-emitting devices. *Applied Physics Letters*, 78(13):1927–1929, 2001.

[23] G. Bjork. On the spontaneous lifetime change in an ideal planar microcavity - transition from a mode continuum to quantized modes. *Ieee Journal of Quantum Electronics*, 30(10):2314–2318, 1994.

[24] D. McBranch, I. H. Campbell, D. L. Smith, and J. P. Ferraris. Optical determination of chain orientation in electroluminescent polymer-films. *Applied Physics Letters*, 66(10):1175–1177, 1995.

[25] R. L. Jones, S. K. Kumar, D. L. Ho, R. M. Briber, and T. P. Russell. Chain conformation in ultrathin polymer films. *Nature*, 400(6740):146–149, 1999.

[26] C. W. Frank, V. Rao, M. M. Despotopoulou, R. F. W. Pease, W. D. Hinsberg, R. D. Miller, and J. F. Rabolt. Structure in thin and ultrathin spin-cast polymer films. *Science*, 273(5277):912–915, 1996.

[27] J. Sturm, S. Tasch, A. Niko, G. Leising, E. Toussaere, J. Zyss, T. C. Kowalczyk, K. D. Singer, U. Scherf, and J. Huber. Optical anisotropy in thin films of a blue electroluminescent conjugated polymer. *Thin Solid Films*, 298(1-2):138–142, 1997.

[28] L. A. A. Pettersson, F. Carlsson, O. Inganas, and H. Arwin. Spectroscopic ellipsometry studies of the optical properties of doped poly(3,4-ethylenedioxythiophene): An anisotropic metal. *Thin Solid Films*, 313:356–361, 1998.

[29] A. P. Monkman, L. E. Horsburgh, M. E. Vaschetto, P. Hatton, H. E. Burrows, W. Brown, and L. A. A. Pettersson. Structure property correlations in a new rigid rod luminescent conjugated polymer polypyridine. *Soc.Plast.Eng*, 57:109–117, 1999.

[30] C. W. Y. Law, K. S. Wong, Z. Yang, L. E. Horsburgh, and A. P. Monkman. Observation of in-plane optical anisotropy of spin-cast rigid- rod electroluminescent polymer films. *Applied Physics Letters*, 76(11):1416–1418, 2000.

[31] J. A. Woollam, P. G. Snyder, and M. C. Rost. Variable angle spectroscopic ellipsometry - a non-destructive characterization technique for ultrathin and multilayer materials. *Thin Solid Films*, 166(1-2):317–323, 1988.

[32] T. W. Lee, O. O. Park, L. M. Do, and T. Zyung. Improvement of el efficiency in polymer light-emitting diodes by heat treatments. *Synthetic Metals*, 117(1-3):249–251, 2001.

[33] M. Redecker, D. D. C. Bradley, M. Inbasekaran, and E. P. Woo. Nondispersive hole transport in an electroluminescent polyfluorene. *Applied Physics Letters*, 73(11):1565–1567, 1998.

[34] M. Grell, W. Knoll, D. Lupo, A. Meisel, T. Miteva, D. Neher, H. G. Nothofer, U. Scherf, and A. Yasuda. Blue polarized electroluminescence from a liquid crystalline polyfluorene. *Advanced Materials*, 11(8):671, 1999.

[35] M. Gross, D. C. Muller, H. G. Nothofer, U. Scherf, D. Neher, C. Brauchle, and K. Meerholz. Improving the performance of doped pi-conjugated polymers for use in organic light-emitting diodes. *Nature*, 405(6787):661–665, 2000.

[36] R. W. T. Higgins, A. P. Monkman, H. G. Nothofer, and U. Scherf. Effects of singlet and triplet energy transfer to molecular dopants in poly-

mer light-emitting diodes and their usefulness in chromaticity tuning. *Applied Physics Letters*, 79(6):857–859, 2001.

[37] R. W. T. Higgins, H. G. Nothofer, U. Scherf, and A. P. Monkman. A study of the energy transfer to porphyrin derivates when used as dopants in polymer light-emitting diodes. *Journal of Applied Physics*, accepted, 2001.

[38] P. A. Lane, L. C. Palilis, D. F. O'Brien, C. Giebeler, A. J. Cadby, D. G. Lidzey, A. J. Campbell, W. Blau, and D. D. C. Bradley. Origin of electrophosphorescence from a doped polymer light emitting diode - art. no. 235206. *Physical Review B*, 6323(23):5206–+, 2001.

[39] T. Virgili, D. G. Lidzey, and D. D. C. Bradley. Efficient energy transfer from blue to red in tetraphenylporphyrin-doped poly(9,9-dioctylfluorene) light-emitting diodes. *Advanced Materials*, 12(1):58, 2000.

[40] C. Rothe, R. Guentner, U. Scherf, and A.P. Monkman. Singlet and triplet energy transfer in a benzil-doped light emitting, solid-state, conjugated polymer. *Journal Of Chemical Physics*, 115(20):9557–9562, 2001.

[41] Steven L. Murov, Gordon L. Hug, and Ian Carmichael. *Handbook of photochemistry*. M. Dekker, New York, 1993.

[42] T. Yamamoto, Y. Miyazaki, T. Fukuda, Z. H. Zhou, T. Maruyama, T. Kanbara, and K. Osakada. Properties and structure of substituted poly(thiophene-2,5- diyl), poly(pyridine-2,5-diyl), and their analogs prepared by organometallic processes. *Synthetic Metals*, 55(2-3):1214–1220, 1993.

[43] M. E. Vaschetto, B. A. Retamal, A. P. Monkman, and M. Springborg. First-principles calculations of pyridines: From monomer to polymer. *Journal of Physical Chemistry A*, 103(50):11096–11103, 1999.

[44] S.J. Broersma. *Journal Of Chemical Physics*, 32:1626, 1960.